Coulomb Excitation of Medium-Weight Even-Even Nuclei*

P. H. Stelson and F. K. McGowan

Oak Ridge National Laboratory, Oak Ridge, Tennessee

(Received December 26, 1957)

The yields of gamma rays resulting from Coulomb excitation have been measured for twenty-nine even-even medium weight nuclei $(92 \leqslant A \leqslant 130)$. The projectiles used for effecting Coulomb excitation were variable-energy protons (1.5 to 3.3 Mev) and doubly-ionized helium ions (8 to 10 Mev). In the most favorable cases the absolute γ-ray yields are determined to an accuracy of $\pm 4\%$. The reduced electric quadrupole transition probabilities, $B(E2)$, are determined to an accuracy of $\pm 7\%$ in favorable cases. For the least favorable case the accuracy is $\pm 20\%$. The observed values for $B(E2)$ are larger than the single particle estimate by factors ranging from 6 to 64. The transition rates in the even-even tin isotopes are larger than the single particle estimate by a factor of 13. A strong correlation is found between the $B(E2)$ and the inverse of the γ-ray energy for transitions with moderately large values for $B(E2)$. The transitions are interpreted in terms of the collective vibrational model. The mass parameters obtained show remarkably little variation and are approximately 10 times the irrotational flow estimate.

I. INTRODUCTION

EARLY work with the Coulomb excitation process showed that low-lying states of medium weight nuclei $(A \sim 100)$ are strongly excited.[1-3] The E2 γ-ray transition rates extracted from the Coulomb excitation cross sections are as much as 50 times larger than the Weisskopf single-particle estimate. These fast transition rates suggest that a collective motion of the nucleons is playing an important role; however, examples of well-developed rotational spectra with their remarkable regularities are not found. Certain regularities, which are less striking than those for rotational spectra, have been discerned in the low-lying states of even-even nuclei of medium weight.[4] The ratio of the positions of the first and second excited states, the spin sequence of the states and the relative transition rates suggest "near harmonic" spectra.[5] Two types of collective motion which generate such spectra have been proposed.[4,6] Recently, the detection of the Coulomb excitation of the second 2+ state in a number of medium-weight nuclei has provided additional information which supports the collective-model interpretation of these states.[7]

In addition to this evidence for the importance of collective motion, it is also apparent that shell structure plays a significant role in the excited states of medium-weight nuclei. This is seen in the rather strong and fairly systematic variation in the energy of the first excited state of even-A nuclei with changes in proton or neutron number. Since E2 transition rates are an unusually sensitive indication of the presence of collec-

tive motion, extensive and accurate information on these transition rates should provide a better understanding of the interplay of the collective-model and shell-model aspects of these states. From the experimental viewpoint, the prospect of making accurate determinations of Coulomb excitation cross sections by γ-ray yield measurements is favorable for medium-weight nuclei. The γ rays have convenient energies; internal conversion is small; and, most important of all, there exists a fairly complete set of isotopically enriched samples with good enrichment factors from which targets may be prepared. In this paper we wish to report the results of Coulomb excitation measurements on 29 even-A medium-weight nuclei.

II. EXPERIMENTAL PROCEDURE

The projectiles used for effecting Coulomb excitation were variable-energy protons and singly- and doubly-ionized helium ions accelerated by the 5.5-Mv ORNL electrostatic generator. The energy spread of the incident particles was approximately 0.1% and the absolute energies were determined to 0.2%. The ion beam current integrator used to determine the number of particles striking the target had an accuracy of better than 0.5% for currents equal to or larger than 0.01 microampere.

Under optimum conditions the ratio He^{++}/He^{+} from the radio-frequency ion source was less than 0.01 and for this reason the beam current of He^{++} was limited to a few hundredths of a microampere. Since He^{++} ions and molecular hydrogen ions have approximately equal e/m values, measures were taken to eliminate hydrogen from the ion source. Even so, a small amount of molecular hydrogen equal to about $\frac{1}{3}$ of the He^{++} current was observed. However, because the e/m values are slightly different we were able to resolve the two beams with the analyzing magnet.

Targets were mounted at 45° with respect to the incident beam on a target support which was a stainless steel tube with 0.005-inch wall thickness. The γ rays resulting from Coulomb excitation were detected with

---

* Work done under the auspices of the U. S. Atomic Energy Commission.

[1] G. M. Temmer and N. P. Heydenburg, Phys. Rev. **98**, 1308 (1955).

[2] P. H. Stelson and F. K. McGowan, Phys. Rev. **99**, 112 (1955).

[3] Mark, McClelland, and Goodman, Phys. Rev. **98**, 1245 (1955).

[4] G. Scharff-Goldhaber and J. Weneser, Phys. Rev. **98**, 212 (1955).

[5] G. Scharff-Goldhaber, Phys. Rev. **103**, 837 (1956).

[6] L. Wilets and M. Jeans, Phys. Rev. **102**, 788 (1956).

[7] P. H. Stelson and F. K. McGowan, Bull. Am. Phys. Soc. Ser. II, **2**, 267 (1957).

thallium activated NaI crystals mounted on DuMont photomultiplier tubes. Two sizes of cylindrical crystals with dimensions $1\frac{1}{2}$ in. diameter—1 in. length and 3 in. diameter—3 in. length were used. Pulse-height spectra were measured with a sliding 20-channel analyzer of ORNL design.[8] The detector was placed at 235° with respect to the incident beam and, usually, with a distance of 10 cm from the target to the front face of the crystal. The prolific x-ray yields produced by proton bombardment were attenuated by placing a series of thin metallic shields in front of the detector.

The energy response of the scintillation spectrometer was calibrated by the use of radioactive sources, e.g., Be[7], Cs[137], Hg[203], which emit γ rays with accurately known energies. To avoid inaccuracy resulting from slight variations in the gain of spectrometer with changes in counting rate, the crystal was simultaneously irradiated by two sources of calibration γ rays and the γ rays from Coulomb excitation.

Metallic targets of normal and enriched isotopic abundance were prepared either by electrodeposition onto 5-mil nickel backings or by sintering metallic powders into thin foils.[9] The sintered foils were mounted on nickel target backing by forming a sandwich of the nickel backing, the foil and a nickel collar; the collar was then spot-welded to the backing. The targets were 75 to 150 mg/cm² in thickness by 0.5 inch in diameter and were, therefore, thick to the impinging projectiles.

In more detail, the various targets were prepared as follows. Enriched targets of ruthenium, palladium, and tin were made directly from the metallic powders obtained from the Stable Isotopes Division by sintering at room temperature under a pressure of 25 tons/in.² The enriched molybdenum isotopes were furnished as oxides. These oxides were reduced to metallic powders by reaction with hydrogen gas at elevated temperatures and then sintered into foils. The enriched cadmium targets were prepared by electrodeposition from cadmium cyanide baths to 95% depletion using a platinum anode. An especially pure target of normal tin was made by electrodeposition from a sodium stannate bath. The target of normal tellurium was made by first depositing a thin layer of lead from a lead fluorobate bath and then depositing the tellurium from a solution of tellurium dioxide in a mixture of hydrofluoric and sulfuric acids. A target of normal zirconium was prepared by spot-welding a 2-mil zirconium (hafnium-free) foil to a nickel backing.

1. Gamma-Ray Spectra

The γ-ray spectra for about 30 different targets of normal and enriched isotopic abundance were measured for a number of incident projectile energies.

In some cases both protons and α particles were used. Representative spectra for these targets are shown in Figs. 1 to 24. The isotopic abundance of the isotope of interest is listed in column 4 of Table II. The spectra for targets enriched in the odd-A isotopes are needed for the complete interpretation of the even-A spectra. These were measured but are not shown here; they are discussed in another paper.[10]

In addition to pulses from γ rays resulting from Coulomb excitation, the spectra contain pulses from (a) the local background, (b) the γ rays from proton bremsstrahlung, and (c) the γ rays from nuclear reactions produced by bombardment of minute amounts of light-element target impurities. Information was previously presented to show that the proton bremsstrahlung is a slowly varying function of the Z of the target material.[2] A tin target was used to obtain the bremsstrahlung spectrum plus local background for the analysis of tellurium, cadmium, palladium, and ruthenium spectra. Since no Coulomb excitation was observed for the enriched Mo[92] target, this spectrum was taken as the proton bremsstrahlung plus local background for the analysis of the other molybdenum spectra. An examination of the representative spectra shows that in favorable cases, e.g., Ru[104] spectrum, the bremsstrahlung plus local background is less than 1% of the peak height of the Coulomb excited γ ray whereas in the least favorable cases, e.g., Te[130] excitation in a normal Te target, the bremsstrahlung plus local background is comparable to the height of the Coulomb excited γ-ray peak. Fortunately, in most spectra the bremsstrahlung intensity is so low that the possible uncertainty in the intensity gives a negligible error in the γ-ray yield.

As is well known, gamma rays from nuclear reactions produced by bombardment of low-Z target impurities cause troublesome interference in Coulomb excitation experiments. For example, the 440-kev γ ray from Na[23](p,p')Na[23] is seen in many of the spectra. To identify these spurious γ rays, the γ-ray spectra of most of the light elements ($Z \leqslant 30$) were measured for a series of proton energies ranging from 1.5- to 4.0-Mev. The presence of target impurities, in addition to producing well-resolved γ-ray peaks, in many cases also raised the continuum level appreciably above the bremsstrahlung level (partly the result of pulses from Compton-recoil electron distributions resulting from higher energy γ rays incident on the detector). In fact, for α-particle spectra, the somewhat irregular continuum from target impurities (see tin spectra) has prevented the definite identification of bremsstrahlung produced by α particles. It was found that preparation of targets by electrodeposition eliminated impurities to a considerable extent. For example, the Cd[114] spectrum has a continuum which is accounted for by the proton bremsstrahlung plus local background.

[8] Kelley, Bell, and Goss, Oak Ridge National Laboratory Physics Division Quarterly Progress Report ORNL-1278, 1951 (unpublished).

[9] The isotopically enriched samples were obtained from the Stable Isotopes Division of Oak Ridge National Laboratory.

[10] F. K. McGowan and P. H. Stelson, Phys. Rev. 109, 901 (1958).

2. Gamma-Ray Yields

The number of emitted γ rays per microcoulomb of incident particles was obtained from the pulse-height spectrum by the use of the formula

$$\mathcal{G} = \frac{N(E_0)}{n(E_0)} \times \frac{1}{\Delta E} \times \frac{1}{\epsilon} \times \frac{1}{R_\gamma} \times \frac{1}{A_\gamma}, \tag{1}$$

where $N(E_0)$ is the counting rate in counts per microcoulomb at the peak of the full-energy peak; $n(E_0) = 1/(a_\gamma \pi^{\frac{1}{2}})$ and a_γ is the half-width of the full-energy peak at $1/e$ amplitude; $\Delta E =$ window width of the pulse-height analyzer; $\epsilon =$ detection efficiency; R_γ is the ratio of the area of the full-energy peak to the total area of the pulse-height spectrum for the γ ray; and A_γ is the correction for absorption of the γ ray by material between the source and crystal.

We now consider the accuracy with which the γ-ray yields are determined by discussing in turn the errors in the quantities on the right-hand side of Eq. (1). The errors given are regarded as standard deviations.

$N(E_0)$.—In favorable cases where the excitation is strong and the isotopic enrichment is high, e.g., Cd^{114} or Ru^{104}, $N(E_0)$ has an error of 1.5%. This results from the statistical and reading error (1%), the channel width error (1%) and the current integrator error (<0.5%). On the other hand, in the least favorable cases the error in $N(E_0)$ may be as much as 15% and is then the principal error in $\mathcal{G}(\gamma\text{'s}/\mu\text{coul})$. These large errors are caused by the combination of relatively weak excitations with strong interference from γ rays excited in the target impurities or in the other isotopes of the target.

$n(E_0)$ or $a_\gamma(E_0)$.—For strong, clean excitations the $a_\gamma(E_0)$ were determined directly from the spectra with an accuracy of 1%. The ratio $a_\gamma(E_0)/E_0$ is a measure of the resolution of the spectrometer and should, in principle, depend only on the γ-ray energy. Therefore, in case of weak excitation or complicated spectra, one can achieve better accuracy by determining $a_\gamma(E_0)$ indirectly from the observed γ-ray energy and the knowledge of the curve $a_\gamma(E_0)/E_0$ vs E_γ. By the use of a series of radioactive sources, we determined this curve to an accuracy of 2% for γ rays with energies of 100-kev to 2000-kev. However, it was found that the resolution for the cases of strong γ rays from Coulomb excitation was slightly poorer (3 to 5% increase in a_γ) than those deduced from the resolution curve obtained from radioactive sources. Further study of this difference showed that it was the result of the large number of soft x-rays present during Coulomb excitation which, after energy degradation to fluorescent x-rays of the graded shield, random sum with the nuclear γ ray being detected. When $a_\gamma(E_0)$ was obtained indirectly by the use of the curve $a_\gamma(E_0)/E_0$ vs E_γ we assigned an error of 3%.

ΔE.—The average window width for the 20 channels,

ΔE, was determined to an accuracy of 0.5%. In addition, there are variations in the individual channel widths of 1% but this is considered as an error in $N(E_0)$.

ϵ.—Values of the total efficiency have been computed by numerical integration for the crystal shapes used for the case of small sources placed at various distances from the crystal surface along the axis of the cylinder.[11] The error in the numerical integration is a few tenths of one percent. The values taken for the cross section (the total cross section minus the coherent scattering cross section) are believed to be known to 1% for the range of γ-ray energies of interest here. The error in the cross section results in a smaller error in ϵ, especially for the 3 in.$\times$3 in. crystals with which most of the measurements were made, because these large crystals are approaching the total absorption condition for γ rays of a few hundred kev energy. For measurements made with the 3 in.$\times$3 in. crystals, the uncertainty in the distance from the target to the front face of the crystal introduces a 1% error in ϵ and an additional 1% error arises from the uncertainty in the dimensions of the crystal. The combination of these errors gives the result that ϵ is known to within 1.5 to 2% for the 3 in.$\times$3 in. crystal. From similar condiderations, the error in ϵ for the $1\frac{1}{2}\times1$ in. crystal is 2 to 3%.

R_γ.—The quantity R_γ, which is defined as the ratio of the area under the full-energy peak to the total area of the γ-ray spectrum, varies with (a) the γ-ray energy, (b) the shape and size of the crystal, and (c) the position of the source with respect to the crystal. Values for R_γ for the 3 in.$\times$3 in. crystal were obtained by measuring spectra of radioactive sources which emit only one γ ray. These spectra were measured with the scintillation counter suspended in the center of a large room to reduce distortion of the spectra at low pulse heights caused by γ rays from the source which first scatter from surrounding objects and then interact with the crystal. The values obtained for R_γ are in good agreement with the results of Lazar, Davis, and Bell,[12] who have made more extensive measurements. We have used their values of R_γ for the $1\frac{1}{2}\times1$ in. crystal. The values for R_γ are believed to be accurate to 3% for both the 3$\times$3 in. and $1\frac{1}{2}\times1$ in. crystals. The way in which formula (1) is written assumes that the full-energy peak is of Gaussian shape. Although this is a very good approximation, it was found that with our 3$\times$3 in. detector as one went far down the high-energy side of the full-energy peak, there occurred a considerable deviation from the Gaussian curve fitted to the peak. The extent of this deviation varied with the γ-ray energy. Consequently, there was a small difference between the actual area under the peak (used in the definition of R_γ) and that given by fitting a Gaussian to the peak. Since Gaussian shapes were assumed in

[11] See P. R. Bell, *Beta- and Gamma-Ray Spectroscopy*, edited by K. Siegbahn (Interscience Publishers, Inc., New York, 1955), p. 132.
[12] Lazar, Davis, and Bell, Nucleonics 14, 52 (1956).

analyzing the Coulomb excitation spectra, a small correction was applied to the values of R_γ to account for this difference in areas.

A_γ.—In our arrangement, the Coulomb-excited γ rays which are detected emerge from the front face of the target, i.e., the face which the beam strikes. Absorption occurs in (1) a small increment of the target itself, (2) the 5-mil stainless steel target holder tube, (3) the x-ray graded shield, (4) the 5-mil aluminum crystal housing, and (5) the thin layer of Al_2O_3 ($\sim$30 mg/cm^2) surrounding the crystal. Although the correction for (1) is appreciable for proton excitation of the low-energy γ rays in the rare-earth region, it is negligible for the γ rays reported here. Absorptions by (2) to (5) are small and may be calculated with fair accuracy. The total absorption for the lowest energy γ ray (Ru^{104}, 358 kev) was less than 4%. The error in $\mathcal{I}$(γ's/μcoul) introduced by the uncertainty in A_γ is thought to be less than 0.5%.

Compounding the errors outlined above, one has the has the result that under the most favorable conditions the absolute γ-ray yield is determined to an accuracy of 4%.

One reason for giving a discussion of the individual sources of error in the γ-ray yields is that the relevant error is different for different applications. For example, one important feature of the γ-ray yields is the variation in yield of a given γ ray with changes in projectile energy. In this case only the error in the area of the full-energy peak is of interest.

The γ-ray yields are given in column 3 of Table I for the corresponding projectile energies listed in column 2. The isotopic abundance of the nucleus of interest is given in column 4 of Table II. The errors given are those for the area of the full-energy peak. The absolute error in the gamma-ray yields may be obtained approximately by combining this error with an additional 4% error (resulting mainly from errors in R_γ and ϵ).

To obtain the reduced electric quadrupole transition probabilities, $B(E2)_{ex}$, one must convert from the γ-ray yields to the number of nuclear excitations. This is done by taking into account (a) the isotopic abundance, i.e., converting to a 100% basis, (b) the total internal-conversion coefficient, α_T, and (c) the angular distribution of the γ rays. The values of α_T were obtained from tables calculated by Rose et al.[13] These values are listed in column 3 of Table II. For the γ rays of interest here, α_T is never more than 2% and since the calculations are fairly accurate, the error in $B(E2)$ caused by the uncertainty in α_T is negligible. In general, the error in the isotopic enrichment is 1% or less.

The γ-ray yields are those for an observation angle of 235°. The angular distribution of the γ rays is of the form $A_0P_0+A_2P_2+A_4P_4$. Since A_2 is always much larger than A_4, the magnitude of the correction for the

angular distribution was minimized by measuring the γ-ray yields at an angle of 235° because P_2 is zero at this angle. A correction for A_4P_4, which is now known both theoretically and experimentally,[14] was applied to the γ-ray yields to obtain A_0. This correction, which depends on E_i, ΔE, Z_2, Z_1, and m (see below for the definition of these quantities) varied from 0 to 10%. The quantities N(excitations/μcoul), are given in column 4 of Table I.

III. EXTRACTION OF $B(E2)_{ex}$

The formula for the cross section for electric quadrupole excitation is

$$\sigma(E2) = \frac{2\pi^2 m^2 V_f^2}{25 Z_2^2 e^2 \hbar^2} B(E2)_{ex} g_{E2}(\xi, \eta_i), \qquad (2)$$

where

$$\xi = \frac{Z_1 Z_2 e^2}{\hbar}\left[\frac{1}{V_f}-\frac{1}{V_i}\right], \quad \eta_i = \frac{Z_1 Z_2 e^2}{\hbar V_i}. \qquad (3)$$

$Z_1 e$ and $Z_2 e$ are the charges of the impinging projectile and the nucleus, respectively. V_i and V_f are the initial and final velocities and m is the reduced mass. $B(E2)$ is the reduced transition probability for excitation by $E2$ radiation. The function $g_{E2}(\xi, \eta_i)$ has been accurately evaluated.[15]

The $B(E2)$ for decay of the 2$^+$ state to the 0$^+$ ground state [denoted by $B(E2)_d$] is equal to $\frac{1}{5}$ the $B(E2)$ for excitation [denoted by $B(E2)_{ex}$]. The values given for $B(E2)$ will actually be those for the quantity $B(E2)/e^2$.

To compare thick target γ-ray yields with theory it is necessary to integrate the theoretical cross section. The [excitations/μcoul], N, of the 2$^+$ state is given by

$$N = \text{const} \int_0^{E_i} \frac{\sigma(E)dE}{S(E)}. \qquad (4)$$

Substituting from Eq. (2) for the cross section gives the result $B(E2)_{ex} \propto N/Y$, where

$$Y = K^2 \int_0^{E_i} \frac{E_f g_{E2}(\xi, \eta_i)dE}{S(E)}. \qquad (5)$$

E_i is the incident energy of the projectile; $E_f = E_i - \Delta E/K$, where ΔE is the energy of the excited state and $K = M_2/(M_1 + M_2)$, M_1 and M_2 being the masses of the projectile and target nuclei, respectively; and $S(E)$ is the rate of energy loss of the projectile in the target.

One of the principal sources of error in the absolute values of $B(E2)$ is the uncertainty in the energy loss of the exciting projectiles in the target materials. For example, one sees from formula (5) that if $S(E)$ is taken uniformly 10% too large, then Y will be in error

[13] Rose, Goertzel, Spinrad, Harr, and Strong, Phys. Rev. 83, 79 (1951), and tables of internal conversion coefficients privately circulated by M. E. Rose.

[14] F. K. McGowan and P. H. Stelson, Phys. Rev. 106, 522 (1957).
[15] See review article by Alder, Bohr, Huus, Mottelson, and Winther, Revs. Modern Phys. 28, 432 (1956).

TABLE I. The nucleus and observed γ-ray energy are given in column 1. Column 3 gives the observed yield of γ rays (at $\theta=55°$) for thick-target bombardment by protons or α particles with energy given in column 2. The errors given are relative errors (see text). The isotopic enrichments of the targets are listed in column 4 of Table II. The yields have not been converted to a 100% isotopic enrichment basis. Column 4 gives the number of excitations per microcoulomb on a 100% isotopic enrichment basis. Corrections for internal conversion (column 3 of Table II) and for the angular distribution were applied to the γ-ray yields to obtain excitations per microcoulomb. Column 5 lists the integral Y (in kev$\times$mg/cm^2) which is needed to deduce the $B(E2)_{ex}$. The integral Y is defined by Eq. (5) in the text. Column 6 lists the $B(E2)_{ex}$ in units of cm^4.

Nucleus (E_γ in kev)	E_p or E_α (Mev)	Yield of γ's/μcoul	Excitations/μcoul	Y	$B(E2)_{ex}$
Mo^{94}(874)	3.00	$(2.48\pm0.25)\times10^4$	$(3.02\pm0.30)\times10^4$	1.41×10^3	$(2.54\pm0.25)\times10^{-49}$
	2.70	$(8.15\pm1.60)\times10^3$	$(9.82\pm1.90)\times10^3$	4.10×10^2	$(2.85\pm0.55)\times10^{-49}$
	2.40	$(1.60\pm0.26)\times10^3$	$(1.91\pm0.31)\times10^3$	7.79×10	$(2.91\pm0.48)\times10^{-49}$
Mo^{96}(775)	3.00	$(5.63\pm0.85)\times10^4$	$(6.33\pm0.95)\times10^4$	2.60×10^3	$(2.89\pm0.44)\times10^{-49}$
	2.70	$(2.20\pm0.33)\times10^4$	$(2.47\pm0.37)\times10^4$	9.40×10^2	$(3.12\pm0.47)\times10^{-49}$
	2.40	$(5.16\pm0.50)\times10^3$	$(5.73\pm0.55)\times10^3$	2.24×10^2	$(3.04\pm0.29)\times10^{-49}$
Mo^{98}(780)	3.00	$(5.17\pm0.35)\times10^4$	$(5.27\pm0.36)\times10^4$	2.51×10^3	$(2.49\pm0.17)\times10^{-49}$
	2.70	$(2.01\pm0.35)\times10^4$	$(2.04\pm0.35)\times10^4$	9.00×10^2	$(2.69\pm0.46)\times10^{-49}$
	2.40	$(5.83\pm0.55)\times10^3$	$(5.86\pm0.55)\times10^3$	2.12×10^2	$(3.28\pm0.30)\times10^{-49}$
Mo^{100}(530)	3.00	$(5.19\pm0.50)\times10^4$	$(5.29\pm0.51)\times10^5$	1.06×10^4	$(5.93\pm0.60)\times10^{-49}$
	2.70	$(2.69\pm0.20)\times10^4$	$(2.72\pm0.20)\times10^5$	5.29×10^3	$(6.10\pm0.48)\times10^{-49}$
	2.40	$(1.13\pm0.10)\times10^4$	$(1.14\pm0.10)\times10^5$	2.12×10^3	$(6.39\pm0.61)\times10^{-49}$
Ru^{96}(840)	3.00	$(2.80\pm0.4\ )\times10^4$	$(2.80\pm0.4\ )\times10^4$	1.52×10^3	$(2.54\pm0.35)\times10^{-49}$
Ru^{98}(654)	3.00	$(1.04\pm0.03)\times10^5$	$(1.55\pm0.05)\times10^5$	$4.9\ \times10^3$	$(4.37\pm0.14)\times10^{-49}$
	2.70	$(4.61\pm0.18)\times10^4$	$(6.83\pm0.27)\times10^4$	2.03×10^3	$(4.65\pm0.18)\times10^{-49}$
	2.40	$(1.54\pm0.08)\times10^4$	$(2.26\pm0.12)\times10^4$	6.18×10^2	$(5.05\pm0.27)\times10^{-49}$
	2.10	$(3.32\pm0.27)\times10^3$	$(4.81\pm0.39)\times10^3$	1.24×10^2	$(5.36\pm0.44)\times10^{-49}$
Ru^{100}(540)	3.00	$(3.34\pm0.09)\times10^5$	$(3.69\pm0.10)\times10^5$	9.40×10^3	$(5.43\pm0.15)\times10^{-49}$
	2.70	$(1.73\pm0.05)\times10^5$	$(1.90\pm0.06)\times10^5$	4.54×10^3	$(5.78\pm0.18)\times10^{-49}$
	2.40	$(7.05\pm0.21)\times10^4$	$(7.67\pm0.23)\times10^4$	1.76×10^3	$(6.02\pm0.18)\times10^{-49}$
	2.10	$(1.84\pm0.15)\times10^4$	$(1.98\pm0.16)\times10^4$	4.81×10^2	$(5.69\pm0.14)\times10^{-49}$
Ru^{102}(475)	3.00	$(6.85\pm0.17)\times10^5$	$(7.19\pm0.18)\times10^5$	1.31×10^4	$(7.59\pm0.19)\times10^{-49}$
	2.70	$(3.37\pm0.09)\times10^5$	$(3.52\pm0.10)\times10^5$	6.83×10^3	$(7.12\pm0.20)\times10^{-49}$
	2.40	$(1.49\pm0.04)\times10^5$	$(1.54\pm0.04)\times10^5$	2.97×10^3	$(7.17\pm0.19)\times10^{-49}$
	2.10	$(4.96\pm0.13)\times10^4$	$(5.09\pm0.13)\times10^4$	9.63×10^2	$(7.30\pm0.19)\times10^{-49}$
	1.80	$(1.03\pm0.03)\times10^4$	$(1.04\pm0.03)\times10^4$	1.91×10^2	$(7.53\pm0.22)\times10^{-49}$
	1.50	$(8.4\ \pm1.3\ )\times10^2$	$(8.35\pm1.3\ )\times10^2$	1.50×10	$(7.69\pm1.2\ )\times10^{-49}$
Ru^{104}(358)	3.00	$(1.49\pm0.04)\times10^6$	$(1.58\pm0.04)\times10^6$	2.31×10^4	$(9.45\pm0.24)\times10^{-49}$
	2.70	$(8.80\pm0.22)\times10^5$	$(9.31\pm0.23)\times10^5$	1.37×10^4	$(9.39\pm0.23)\times10^{-49}$
	2.40	$(4.39\pm0.11)\times10^5$	$(4.61\pm0.11)\times10^5$	7.14×10^3	$(8.92\pm0.21)\times10^{-49}$
	2.10	$(1.94\pm0.05)\times10^5$	$(2.02\pm0.05)\times10^5$	3.04×10^3	$(9.18\pm0.23)\times10^{-49}$
	1.80	$(6.11\pm0.16)\times10^4$	$(6.30\pm0.16)\times10^4$	9.19×10^2	$(9.47\pm0.24)\times10^{-49}$
	1.50	$(1.01\pm0.03)\times10^4$	$(1.03\pm0.03)\times10^4$	1.54×10^2	$(9.24\pm0.29)\times10^{-49}$
Pd^{104}(555)	3.30	$(3.21\pm0.10)\times10^5$	$(5.08\pm0.16)\times10^5$	1.43×10^4	$(5.63\pm0.18)\times10^{-49}$
	2.40	$(2.80\pm0.10)\times10^4$	$(4.35\pm0.17)\times10^4$	1.32×10^3	$(5.22\pm0.16)\times10^{-49}$
	2.10	$(7.45\pm0.30)\times10^3$	$(1.15\pm0.05)\times10^4$	3.28×10^2	$(5.56\pm0.17)\times10^{-49}$
Pd^{106}(513)	3.30	$(6.21\pm0.15)\times10^5$	$(7.47\pm0.18)\times10^5$	1.81×10^4	$(6.54\pm0.16)\times10^{-49}$
	3.00	$(3.34\pm0.10)\times10^5$	$(4.00\pm0.12)\times10^5$	1.03×10^4	$(6.16\pm0.19)\times10^{-49}$
	2.70	$(1.66\pm0.05)\times10^5$	$(1.98\pm0.06)\times10^5$	5.03×10^3	$(6.24\pm0.20)\times10^{-49}$
	2.40	$(6.73\pm0.16)\times10^4$	$(7.95\pm0.19)\times10^4$	1.91×10^3	$(6.60\pm0.16)\times10^{-49}$
	2.10	$(1.98\pm0.05)\times10^4$	$(2.32\pm0.06)\times10^4$	5.34×10^2	$(6.89\pm0.18)\times10^{-49}$
Pd^{108}(433)	3.30	$(1.12\pm0.03)\times10^6$	$(1.19\pm0.03)\times10^6$	2.50×10^4	$(7.53\pm0.20)\times10^{-49}$
	3.00	$(6.66\pm0.18)\times10^5$	$(7.02\pm0.19)\times10^5$	1.50×10^4	$(7.42\pm0.20)\times10^{-9}$
	2.70	$(3.58\pm0.08)\times10^5$	$(3.76\pm0.08)\times10^5$	8.00×10^3	$(7.45\pm0.16)\times10^{-49}$
	2.40	$(1.59\pm0.04)\times10^5$	$(1.66\pm0.04)\times10^5$	3.62×10^3	$(7.27\pm0.17)\times10^{-49}$
	2.10	$(7.53\pm0.24)\times10^4$	$(7.80\pm0.25)\times10^4$	1.24×10^3	$(9.95\pm0.35)\times10^{-49}$
Pd^{110}(374)	3.30	$(1.65\pm0.04)\times10^6$	$(1.82\pm0.04)\times10^6$	3.22×10^4	$(8.95\pm0.20)\times10^{-49}$
	3.00	$(1.01\pm0.02)\times10^6$	$(1.11\pm0.02)\times10^6$	2.03×10^4	$(8.67\pm0.16)\times10^{-49}$
	2.70	$(5.62\pm0.12)\times10^5$	$(6.15\pm0.13)\times10^5$	1.15×10^4	$(8.72\pm0.18)\times10^{-49}$
	2.40	$(2.87\pm0.10)\times10^5$	$(3.12\pm0.11)\times10^5$	5.93×10^3	$(8.34\pm0.29)\times10^{-49}$
	2.10	$(1.11\pm0.03)\times10^5$	$(1.20\pm0.03)\times10^5$	2.37×10^3	$(8.03\pm0.20)\times10^{-49}$
Cd^{106}(630)	3.30	$(8.96\pm0.45)\times10^4$	$(2.67\pm0.13)\times10^5$	9.45×10^3	$(5.14\pm0.25)\times10^{-49}$
	3.00	$(3.95\pm0.30)\times10^4$	$(1.17\pm0.09)\times10^5$	4.64×10^3	$(4.58\pm0.36)\times10^{-49}$
	2.70	$(1.49\pm0.15)\times10^4$	$(4.38\pm0.44)\times10^4$	1.88×10^3	$(4.24\pm0.43)\times10^{-49}$
	2.40	$(5.43\pm0.80)\times10^3$	$(1.58\pm0.23)\times10^4$	5.46×10^2	$(5.26\pm0.77)\times10^{-49}$
	2.10	$(6.25\pm1.50)\times10^2$	$(1.81\pm0.45)\times10^3$	1.02×10^2	$(3.23\pm0.80)\times10^{-49}$

TABLE I.—*Continued*.

Nucleus (E_γ in kev)	E_p or E_α (Mev)	Yield of γ's/μcoul	Excitations/μcoul	Y	$B(E2)_{ex}$
Cd^{108}(630)	3.30	$(5.43\pm1.00)\times10^4$	$(3.75\pm0.69)\times10^5$	9.45×10^3	$(7.21\pm1.3\ )\times10^{-49}$
	3.00	$(1.97\pm0.35)\times10^4$	$(1.35\pm0.24)\times10^5$	4.64×10^3	$(5.29\pm0.96)\times10^{-49}$
	2.70	$(6.11\pm1.20)\times10^3$	$(4.16\pm0.82)\times10^4$	1.88×10^3	$(4.02\pm0.80)\times10^{-49}$
	2.40	$(2.17\pm0.50)\times10^3$	$(1.45\pm0.34)\times10^4$	5.46×10^2	$(4.83\pm1.14)\times10^{-49}$
Cd^{110}(656)	3.30	$(1.65\pm0.04)\times10^5$	$(2.30\pm0.06)\times10^5$	8.14×10^3	$(5.14\pm0.13)\times10^{-49}$
	3.00	$(7.52\pm0.19)\times10^4$	$(1.04\pm0.03)\times10^5$	3.92×10^3	$(4.82\pm0.14)\times10^{-49}$
	2.70	$(2.99\pm0.15)\times10^4$	$(4.12\pm0.21)\times10^4$	1.54×10^3	$(4.86\pm0.25)\times10^{-49}$
	2.40	$(9.20\pm0.50)\times10^3$	$(1.26\pm0.07)\times10^4$	4.19×10^2	$(5.47\pm0.30)\times10^{-49}$
	2.10	$(1.46\pm0.08)\times10^3$	$(1.98\pm0.09)\times10^3$	7.26×10	$(5.03\pm0.23)\times10^{-49}$
Cd^{112}(610)	3.30	$(2.68\pm0.08)\times10^5$	$(3.14\pm0.09)\times10^5$	1.05×10^4	$(5.44\pm0.16)\times10^{-49}$
	3.00	$(1.28\pm0.03)\times10^5$	$(1.49\pm0.04)\times10^5$	5.27×10^3	$(5.14\pm0.14)\times10^{-49}$
	2.70	$(5.73\pm0.14)\times10^4$	$(6.65\pm0.16)\times10^4$	2.18×10^3	$(5.55\pm0.13)\times10^{-49}$
	2.40	$(1.79\pm0.06)\times10^4$	$(2.06\pm0.07)\times10^4$	6.71×10^2	$(5.58\pm0.19)\times10^{-49}$
	2.10	$(3.43\pm0.16)\times10^3$	$(3.92\pm0.18)\times10^3$	1.33×10^2	$(5.36\pm0.25)\times10^{-49}$
Cd^{114}(555)	3.30	$(4.30\pm0.10)\times10^5$	$(4.50\pm0.10)\times10^5$	1.38×10^4	$(6.11\pm0.14)\times10^{-49}$
	3.00	$(2.14\pm0.05)\times10^5$	$(2.23\pm0.05)\times10^5$	7.30×10^3	$(5.55\pm0.12)\times10^{-49}$
	2.70	$(1.02\pm0.02)\times10^5$	$(1.05\pm0.02)\times10^5$	3.30×10^3	$(5.78\pm0.11)\times10^{-49}$
	2.40	$(3.61\pm0.09)\times10^4$	$(3.70\pm0.09)\times10^4$	1.16×10^3	$(5.80\pm0.14)\times10^{-49}$
	2.10	$(8.71\pm0.27)\times10^3$	$(8.86\pm0.28)\times10^3$	2.67×10^2	$(6.03\pm0.19)\times10^{-49}$
	9.00[a]	$(2.03\pm0.05)\times10^6$	$(2.13\pm0.05)\times10^6$	3.46×10^4	$(5.60\pm0.14)\times10^{-49}$
Cd^{116}(517)	3.30	$(3.85\pm0.09)\times10^5$	$(5.44\pm0.13)\times10^5$	1.66×10^4	$(5.96\pm0.14)\times10^{-49}$
	3.00	$(2.16\pm0.05)\times10^5$	$(3.05\pm0.07)\times10^5$	9.16×10^3	$(6.05\pm0.14)\times10^{-49}$
	2.70	$(1.03\pm0.03)\times10^4$	$(1.37\pm0.04)\times10^5$	4.33×10^3	$(5.75\pm0.17)\times10^{-49}$
	2.40	$(4.00\pm0.10)\times10^4$	$(5.45\pm0.14)\times10^4$	1.63×10^3	$(6.08\pm0.16)\times10^{-49}$
	2.10	$(1.14\pm0.03)\times10^4$	$(1.54\pm0.04)\times10^4$	4.33×10^2	$(6.47\pm0.17)\times10^{-49}$
Te^{126}(673)	3.30	$(2.59\pm0.25)\times10^4$	$(1.40\pm0.13)\times10^5$	6.45×10^3	$(5.25\pm0.50)\times10^{-49}$
	3.00	$(1.18\pm0.12)\times10^4$	$(6.11\pm0.62)\times10^4$	2.89×10^3	$(5.12\pm0.50)\times10^{-49}$
	10.00[a]	$(3.26\pm0.11)\times10^5$	$(1.73\pm0.06)\times10^6$	3.83×10^4	$(5.47\pm0.20)\times10^{-49}$
	9.00[a]	$(1.76\pm0.06)\times10^5$	$(9.33\pm0.33)\times10^5$	2.07×10^4	$(5.45\pm0.20)\times10^{-49}$
Te^{128}(750)	3.30	$(2.14\pm0.20)\times10^4$	$(6.51\pm0.65)\times10^4$	4.08×10^3	$(3.87\pm0.38)\times10^{-49}$
	3.00	$(9.22\pm1.00)\times10^3$	$(2.79\pm0.30)\times10^4$	1.62×10^3	$(4.17\pm0.43)\times10^{-49}$
	10.00[a]	$(3.25\pm0.11)\times10^5$	$(1.01\pm0.04)\times10^6$	2.95×10^4	$(4.14\pm0.14)\times10^{-49}$
	9.00[a]	$(1.71\pm0.06)\times10^5$	$(5.32\pm0.19)\times10^5$	1.50×10^4	$(4.29\pm0.15)\times10^{-49}$
Te^{130}(850)	3.30	$(9.40\pm0.80)\times10^3$	$(2.63\pm0.22)\times10^4$	2.10×10^3	$(3.03\pm0.30)\times10^{-49}$
	3.00	$(4.04\pm0.60)\times10^3$	$(1.72\pm0.13)\times10^4$	7.31×10^2	$(3.71\pm0.70)\times10^{-49}$
	10.00[a]	$(2.02\pm0.09)\times10^5$	$(5.77\pm0.26)\times10^5$	2.10×10^4	$(3.33\pm0.15)\times10^{-49}$
	9.00[a]	$(9.97\pm0.45)\times10^4$	$(2.85\pm0.13)\times10^5$	9.95×10^3	$(3.47\pm0.15)\times10^{-49}$
Sn^{116}(1268)	9.13[a]	$(4.02\pm0.37)\times10^4$	$(4.23\pm0.39)\times10^4$	2.03×10^3	$(2.17\pm0.20)\times10^{-49}$
	10.13[a]	$(1.03\pm0.09)\times10^5$	$(1.08\pm0.09)\times10^5$	5.72×10^3	$(1.97\pm0.17)\times10^{-49}$
Sn^{118}(1219)	8.12[a]	$(1.44\pm0.21)\times10^4$	$(1.48\pm0.21)\times10^4$	6.95×10^2	$(2.21\pm0.32)\times10^{-49}$
	9.13[a]	$(5.64\pm0.41)\times10^4$	$(5.80\pm0.42)\times10^4$	2.56×10^3	$(2.35\pm0.17)\times10^{-49}$
	10.13[a]	$(1.45\pm0.07)\times10^5$	$(1.50\pm0.07)\times10^5$	6.88×10^3	$(2.28\pm0.12)\times10^{-49}$
Sn^{120}(1155)	8.12[a]	$(2.31\pm0.27)\times10^4$	$(2.29\pm0.27)\times10^4$	9.85×10^2	$(2.43\pm0.28)\times10^{-49}$
	9.13[a]	$(7.52\pm0.36)\times10^4$	$(7.50\pm0.36)\times10^4$	3.39×10^3	$(2.30\pm0.11)\times10^{-49}$
	10.13[a]	$(1.75\pm0.07)\times10^5$	$(1.75\pm0.07)\times10^4$	8.72×10^3	$(2.09\pm0.08)\times10^{-49}$
Sn^{122}(1130)	8.12[a]	$(3.36\pm0.45)\times10^4$	$(3.60\pm0.47)\times10^4$	1.13×10^3	$(3.31\pm0.43)\times10^{-49}$
	9.13[a]	$(9.78\pm0.93)\times10^4$	$(1.05\pm0.99)\times10^5$	3.80×10^3	$(2.88\pm0.27)\times10^{-49}$
	10.13[a]	$(1.97\pm0.16)\times10^5$	$(2.12\pm0.16)\times10^5$	9.56×10^3	$(2.33\pm0.17)\times10^{-49}$
Sn^{124}(1128)	8.12[a]	$(2.61\pm0.34)\times10^4$	$(2.73\pm0.35)\times10^4$	1.15×10^3	$(2.48\pm0.31)\times10^{-49}$
	9.13[a]	$(6.87\pm0.47)\times10^4$	$(7.20\pm0.50)\times10^4$	3.85×10^3	$(1.95\pm0.13)\times10^{-49}$
	10.13[a]	$(1.81\pm0.12)\times10^5$	$(1.92\pm0.12)\times10^5$	9.66×10^3	$(2.06\pm0.13)\times10^{-49}$
Zr^{92,94}(920)	9.00[a]	$(7.17\pm0.72)\times10^4$	$(2.05\pm0.21)\times10^5$	1.33×10^4	$(0.79\pm0.08)\times10^{-49}$

[a] Doubly charged α particles.

by 10%. The existing information on $S(E)$ for medium-weight elements for protons and α particles of several Mev energy has an estimated accuracy of 10%. Since the yield of γ rays, $\mathcal{G}$, which is the other main source of error in obtaining $B(E2)$, can in some cases be measured to 4%, the error in $S(E)$ is seen to be quite important. In the limit of very thin targets the uncertainty is $S(E)$ is eliminated. However, it has been impractical to con-

TABLE II. Column 2 lists the observed γ-ray energy from Coulomb excitation of the target nucleus in column 1. The assigned error is considered to be a standard deviation. Columns 3 and 4 list the total internal conversion coefficient and the isotopic enrichment of the target. Column 5 lists our best value for the $B(E2)_{ex}$ in units cm^4 (converted to a 100% isotopic abundance basis). The columns headed R.E. and A.E. give, respectively, the relative percentage error (see text) and the absolute percentage error (standard deviations) for the $B(E2)_{ex}$. The column headed $B(E2)_d/B(E2)_{sp}$ contains the ratio of the observed decay rate to that for a single-particle transition. The quantities β, C_2, and $B_2/(B_2)_{irrot}$, which are listed in the last three columns, are defined in the text.

Nucleus	E (kev)	αT	Isotopic abundance	$B(E2)_{ex}$ $\times 10^{49}$	R.E.	A.E.	$\dfrac{B(E2)_d}{B(E2)_{sp}}$	$T_{\frac{1}{2}}$ (sec)	β	C_2 (Mev)	$B_2/(B_2)_{irrot}$
Mo^{94}	874$\pm$ 9	0.0011	79.1 $\pm$1.0	2.70	$\pm$11	$\pm$13	21	2.0$\times$10^{-12}	0.174	72	12
Mo^{96}	775$\pm$ 8	0.0015	85.94$\pm$1.0	3.02	$\pm$11	$\pm$13	23	3.4$\times$10^{-12}	0.181	59	12
Mo^{98}	780$\pm$ 8	0.0015	95.0 $\pm$1.0	2.70	$\pm$10	$\pm$12	20	3.6$\times$10^{-12}	0.169	68	13
Mo^{100}	530$\pm$ 5	0.0038	9.67^a	6.14	$\pm$ 8	$\pm$10	48	1.1$\times$10^{-11}	0.252	21	8.4
Ru^{96}	840$\pm$10	0.0017	95.51$\pm$0.11	2.54	$\pm$15	$\pm$16	19	2.7$\times$10^{-12}	0.160	83	14
Ru^{98}	654$\pm$ 6	0.0032	65.1 $\pm$0.4	4.75	$\pm$ 6	$\pm$ 8	35	5.0$\times$10^{-12}	0.214	36	9.8
Ru^{100}	540$\pm$ 5	0.0052	88.9 $\pm$0.1	5.72	$\pm$ 5	$\pm$ 7	41	1.1$\times$10^{-11}	0.232	25	9.6
Ru^{102}	475$\pm$ 5	0.0076	94.24$\pm$0.03	7.33	$\pm$ 4	$\pm$ 7	52	1.6$\times$10^{-11}	0.259	17.7	8.5
Ru^{104}	358$\pm$ 3	0.0188	95.1 $\pm$0.2	9.28	$\pm$ 4	$\pm$ 7	64	5.2$\times$10^{-11}	0.276	10.8	8.9
Pd^{104}	555$\pm$ 6	0.0045	62.20$\pm$2.43	5.47	$\pm$ 5	$\pm$ 7	38	9.8$\times$10^{-12}	0.214	31	10.6
Pd^{106}	513$\pm$ 5	0.0056	82.33$\pm$0.03	6.46	$\pm$ 5	$\pm$ 7	43	1.2$\times$10^{-11}	0.227	25	9.7
Pd^{108}	433$\pm$ 4	0.0087	94.19$\pm$0.11	7.42	$\pm$ 4	$\pm$ 7	48	2.5$\times$10^{-11}	0.241	18.8	9.9
Pd^{110}	374$\pm$ 4	0.0137	91.42$\pm$0.32	8.60	$\pm$ 4	$\pm$ 7	55	4.5$\times$10^{-11}	0.255	14.4	9.9
Cd^{106}	630$\pm$10	0.0036	32.9 $\pm$0.5	4.70	$\pm$ 9	$\pm$11	32	6.0$\times$10^{-12}	0.186	46	12
Cd^{108}	630$\pm$10	0.0036	14.2 $\pm$0.2	5.35	$\pm$20	$\pm$21	35	5.3$\times$10^{-12}	0.195	41	10
Cd^{110}	656$\pm$ 6	0.0032	70.0 $\pm$0.5	5.04	$\pm$ 6	$\pm$ 8	32	4.6$\times$10^{-12}	0.187	47	10.4
Cd^{112}	610$\pm$ 6	0.0039	83.5 $\pm$1.0	5.42	$\pm$ 5	$\pm$ 7	34	6.2$\times$10^{-12}	0.193	42	10.5
Cd^{114}	555$\pm$ 5	0.0050	94.2 $\pm$1.0	5.84	$\pm$ 4	$\pm$ 7	35	9.2$\times$10^{-12}	0.197	36	10.5
Cd^{116}	517$\pm$ 5	0.0061	71.2 $\pm$0.5	6.00	$\pm$ 4	$\pm$ 7	36	1.3$\times$10^{-11}	0.197	33	10.8
Te^{126}	673$\pm$ 7	0.0032	18.69^a	5.32	$\pm$ 5	$\pm$ 7	28	3.8$\times$10^{-12}	0.163	64	11
Te^{128}	750$\pm$10	0.0024	31.81^a	4.12	$\pm$ 6	$\pm$ 8	21	2.9$\times$10^{-12}	0.141	94	12
Te^{130}	850$\pm$10	0.0018	34.44^a	3.40	$\pm$ 7	$\pm$ 9	17	1.9$\times$10^{-12}	0.127	130	13
Sn^{116}	1268$\pm$10	0.0008	92.64$\pm$0.07	2.07	$\pm$11	$\pm$13	12	4.2$\times$10^{-13}	0.111	260	14
Sn^{118}	1219$\pm$10	0.0009	94.91$\pm$0.19	2.28	$\pm$10	$\pm$12	13	4.6$\times$10^{-13}	0.115	230	13
Sn^{120}	1155$\pm$10	0.0010	98.14$\pm$0.07	2.20	$\pm$ 8	$\pm$10	13	6.3$\times$10^{-13}	0.112	230	14
Sn^{122}	1130$\pm$10	0.0010	88.92$\pm$0.06	2.52	$\pm$10	$\pm$12	14	6.0$\times$10^{-13}	0.119	200	13
Sn^{124}	1128$\pm$10	0.0010	90.26$\pm$0.06	2.13	$\pm$ 9	$\pm$11	12	7.9$\times$10^{-13}	0.108	240	16
Zr$^{92, 94}$	920$\pm$10	0.0009	34.5^a	0.79	$\pm$11	$\pm$13	6.3	5.5$\times$10^{-12}	0.100	230	23

^{a} Targets with natural isotopic abundance.

struct thin targets of accurately known thickness from the limited amounts of enriched isotopes available. In order to reduce the error in $B(E2)$ from the uncertainty in $S(E)$ for thick-target experiments, measurements were made with thick and thin targets of silver $(Z=47)$ and gold $(Z=79)$, since for these two elements one can make stable uniform thin targets of accurately known thickness. From a comparison of the values for $B(E2)$ obtained from thin and thick targets for a series of incident energies, one can deduce the error in $S(E)$ and alter $S(E)$ until the yields from thin and thick targets give consistent values for $B(E2)$. The details of these experiments are given in the appendix. It is believed that the error in $S(E)$ for protons in silver has been reduced to 4%. The new values are approximately 10% larger than those previously used.[2] The stopping power for α particles in silver was obtained using the assumption that $S_\alpha = 4S_p$ at an α-particle energy which is 4 times the proton energy. The resulting values for $S(E)_\alpha$ are in good agreement with the early measurements of Rosenblum.[16] The stopping power of silver was

used to obtain the stopping power of other medium weight elements on the assumption that $S(E)$ expressed in kev/mg/cm^2 varies as $Z^{-\frac{1}{3}}$. This procedure ignores "shell effects" which might be as large as several percent.[17]

Other sources of error in the values for $B(E2)_{ex}$ result from errors in (a) the incident energy, E_i, (b) the excitation energy of the state, ΔE, and (c) the actual numerical evaluation of the integrals, Y. The integrals are quite sensitive to changes in E_i and ΔE. For example, in the least favorable cases, e.g., α-particle excitation of the tin states, a 1% alteration of E_i changes Y by 5 to 10% and a 1% alteration of ΔE changes Y by 5%. In the most favorable cases, e.g., proton excitation of Ru^{104}, a 1% alteration of E_i changes Y by 5% and a 1% alteration of ΔE changes Y by 2%. Since we have determined the incident energies to 0.2%, the errors in $B(E2)_{ex}$ resulting from errors in E_i are 1 to 2%. In general the excitation energies have an accuracy of about 1% which means the resulting errors in $B(E2)_{ex}$ range from 2 to 5%. The integrals, Y, were obtained

[16] S. Rosenblum, Ann. phys. 10, 408 (1928).

[17] A. Winther (private communication).

from numerical integrations by the use of Simpson's rule. It is believed that they are correct to within 2%; the uncertainty results in part from the actual numerical integration and in part from reading and interpolation errors in $g_{E2}(\xi,\eta_i)$.

The values for the integrals, Y, in units of $\mathrm{kev} \times \mathrm{mg/cm^2}$, are given in column 5 of Table I. The last column contains the values for $B(E2)_{\mathrm{ex}}$ deduced from the $N(\mathrm{excitations}/\mu\mathrm{coul})$ and Y. The errors listed for the $B(E2)_{\mathrm{ex}}$ in this table reflect only the error in the area of the full-energy γ-ray peak since we are interested here in the constancy of $B(E2)_{\mathrm{ex}}$ for different bombarding energies.
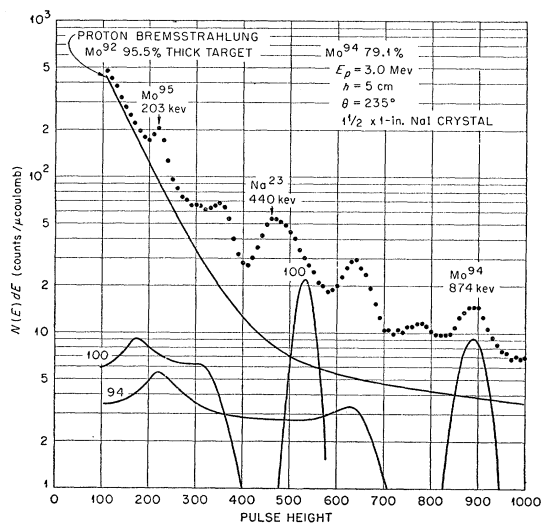
FIG. 1. Pulse-height spectrum for 3.0-Mev protons on Mo⁹⁴ target. The curve labeled proton bremsstrahlung also includes local background. The curve labeled 100 (for Mo¹⁰⁰) and the peak labeled Mo⁹⁵ indicate the contributions from Coulomb excitation of these isotopes in the enriched Mo⁹⁴ target.
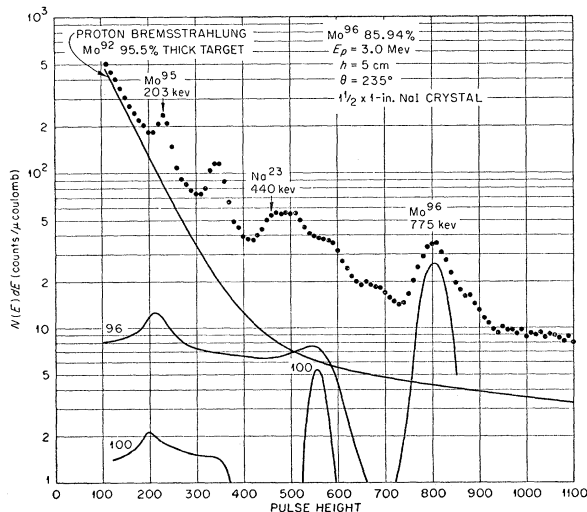
FIG. 2. Pulse-height spectrum for protons on Mo⁹⁶ target.
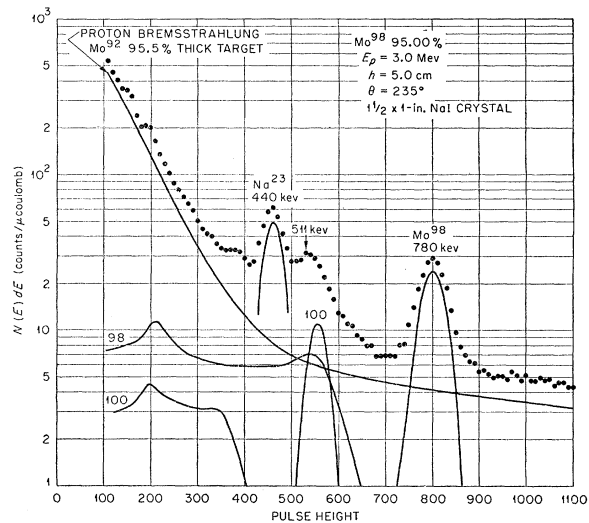
FIG. 3. Pulse-height spectrum for protons on Mo⁹⁸ target.
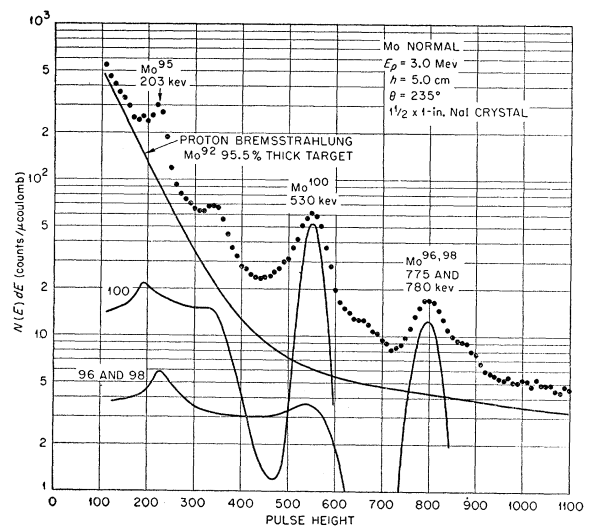
FIG. 4. Pulse-height spectrum for protons on normal molybdenum target.

Our best values for the $B(E2)_{\mathrm{ex}}$ are given in column 5 of Table II. The columns headed R.E. and A.E. list percentage errors assigned to the $B(E2)_{\mathrm{ex}}$. The relative error (R.E.) includes all the errors discussed above in $N(\mathrm{excitations}/\mu\mathrm{coul})$ and in Y which enter into the comparison of the relative transition rates for the different nuclei. The absolute percentage error (A.E.) contains additional sources of error (mainly the error in the absolute stopping power) which are common to all the transitions measured.

IV. REMARKS ON INDIVIDUAL CASES

A. Zirconium $(Z=40)$.—The γ-ray spectrum resulting from 9-Mev α-particle bombardment of a normal zirconium target is shown in Fig. 21. Both Zr⁹² and Zr⁹⁴ are known to have first excited states at 920 kev
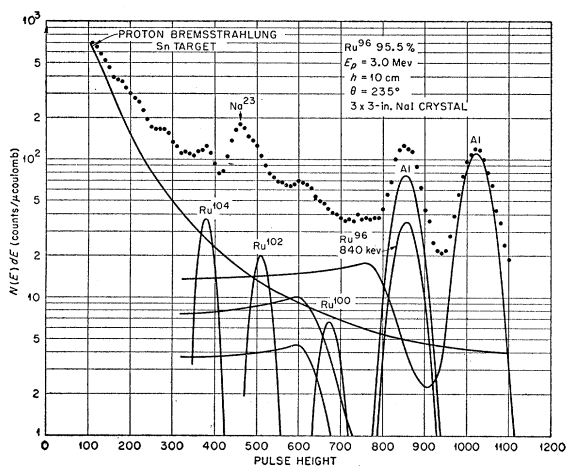
FIG. 5. Pulse-height spectrum for protons on Ru^{96} target.
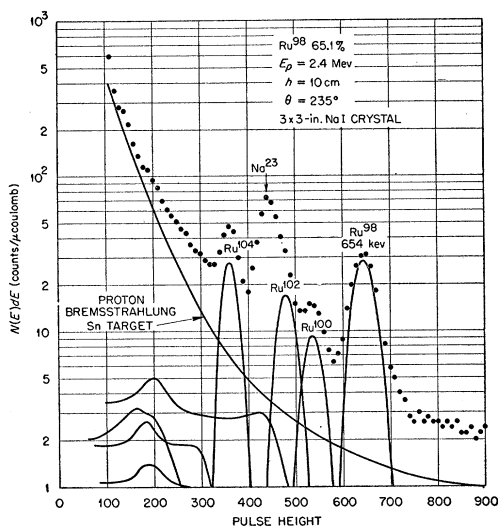
FIG. 6. Pulse-height spectrum for protons on Ru^{98} target.

from other types of experiments.[18] Therefore, the 920-kev γ ray is interpreted as resulting from Coulomb excitation of the first excited state of both nuclei and the $B(E2)_{ex}$ is the average for the two transitions.

B. *Molybdenum* $(Z=42)$.—Figures 1 to 4 show spectra obtained from 3.0-Mev proton bombardment of targets enriched in Mo^{94}, Mo^{96}, Mo^{98}, and normal molybdenum, respectively. The normal molybdenum target was used to obtain the $B(E2)_{ex}$ for Mo^{100} because insufficient enriched Mo^{100} was available. We had previously reported the energy of the first excited state of Mo^{100} as (540 ± 7) kev[2]; a somewhat more accurate measurement, made in the manner described above, gives (530 ± 5) kev.

A 320-kev γ ray is observed in several of the spectra (it is especially strong in Mo^{96}), and a 620-kev γ ray is seen in the Mo^{94} spectrum. We believe that these γ rays do not result from Coulomb excitation of

molybdenum but we are not able to identify the reactions producing these γ rays. We have determined that both γ rays are in coincidence with hard radiation (>1 Mev) which eliminates the possibility that they result from Coulomb excitation of molybdenum.

The positions of the excited states and the $B(E2)_{ex}$ for the four molybdenum isotopes agree well with those obtained by Temmer and Heydenburg who studied the Coulomb excitation of these isotopes by the use of α particles.[19]

C. *Ruthenium* $(Z=44)$.—Figures 5 to 9 show representative spectra for proton excitation of enriched samples of Ru^{96}, Ru^{98}, Ru^{100}, Ru^{102}, and Ru^{104}, respectively. The γ ray from the weak excitation of the 840-kev
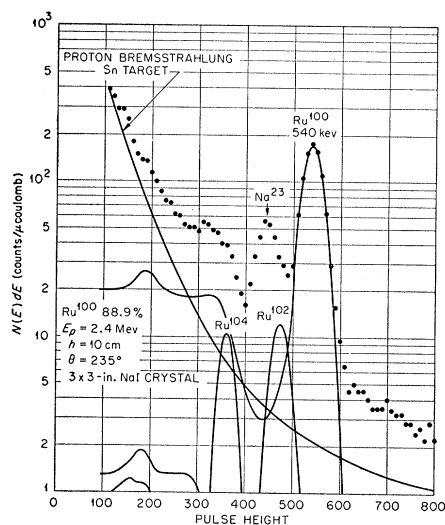
FIG. 7. Pulse-height spectrum for protons on Ru^{100} target.
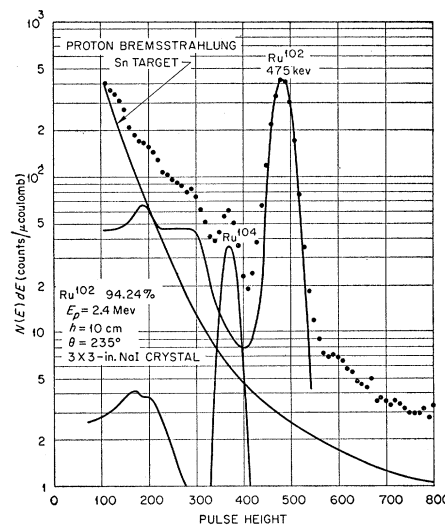
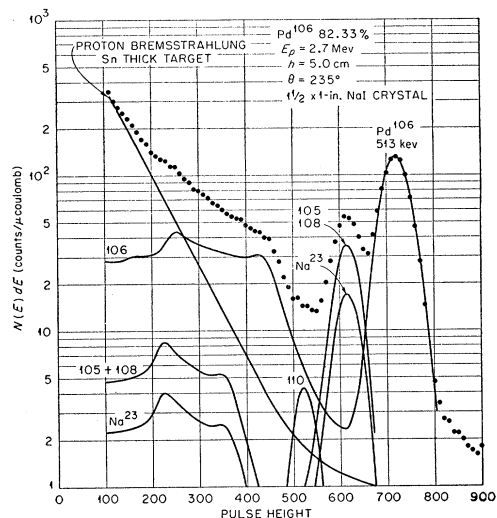FIG. 8. Pulse-height spectrum for protons on Ru^{102} target.

[18] G. L. Griffith, Phys. Rev. **103**, 643 (1956); Hayward, Hopper, and Ernst, Phys. Rev. **98**, 231(A) (1955).

[19] G. T. Temmer and N. P. Heydenburg, Phys. Rev. **104**, 967 (1956).

state in Ru^{96} is superimposed on a γ ray of the same energy resulting from the $Al(p,p'\gamma)$ reaction in a 0.15% target impurity of aluminum. The $Al(p,p'\gamma)$ reaction also produces a strong γ ray of 1010 kev. By the measurement of the intensity of these two γ rays from proton bombardment of aluminum, it was possible, by normalizing to the 1010-kev peak, to infer the fraction of the 840-kev peak caused by the aluminum γ ray. This is shown in Fig. 5.

The values of $B(E2)_{ex}$ for the 475-kev state of Ru^{102} showed a considerable increase at the lower proton bombarding energies. We have concluded that this was caused by a small amount of lithium in the target ($\sim$5 ppm by weight). The high yield of 478-kev γ rays from the $Li^7(p,p'\gamma)$ reaction increases much more slowly with increasing proton energy than does the
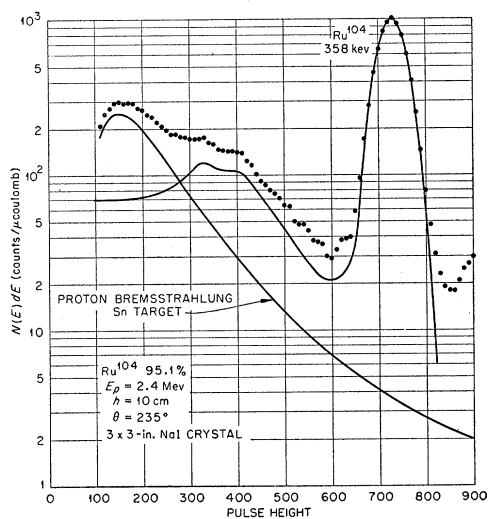
FIG. 9. Pulse-height spectrum for protons on Ru^{104} target.
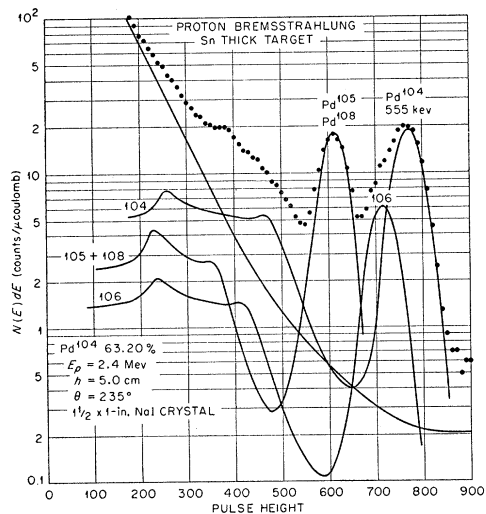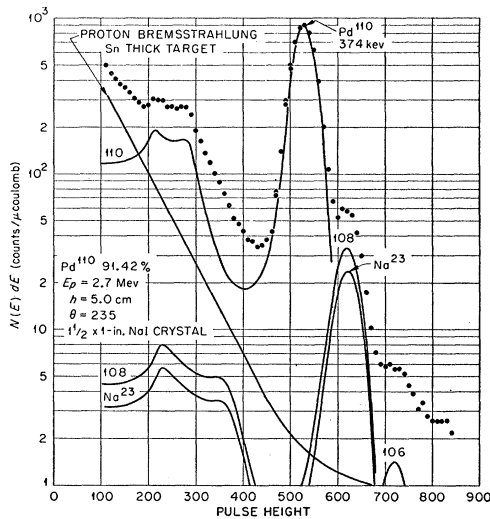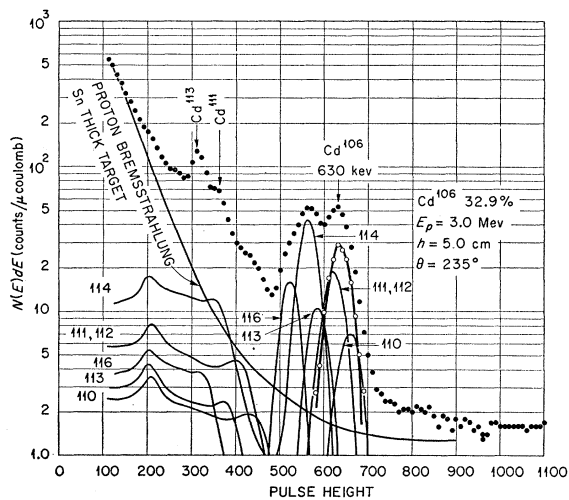

FIG. 10. Pulse-height spectrum for protons on Pd^{104} target.

FIG. 11. Pulse-height spectrum for protons on Pd^{106} target.
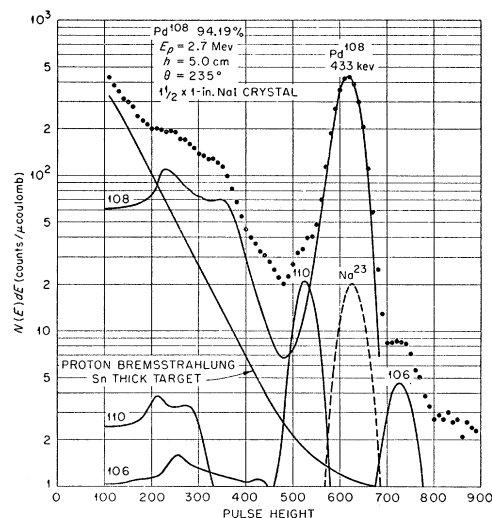
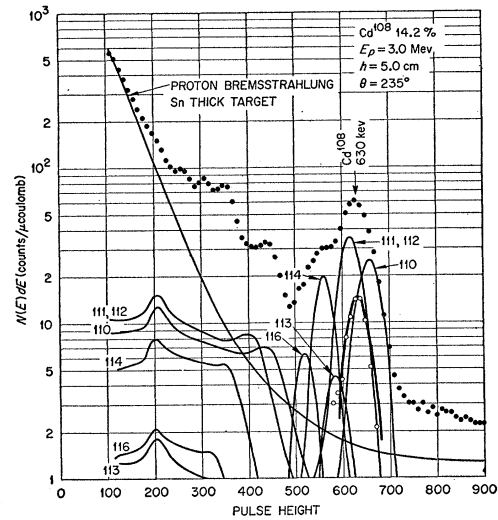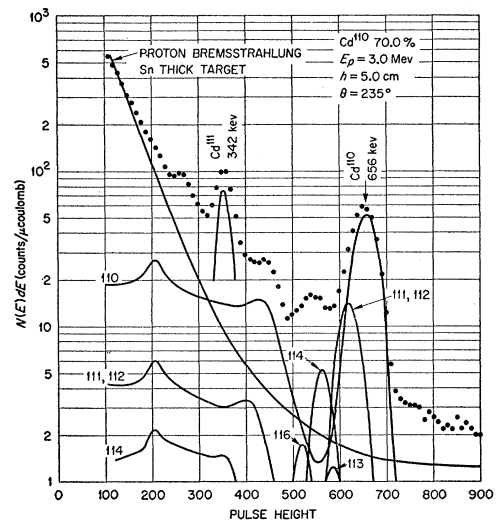FIG. 12. Pulse-height spectrum for protons on Pd^{108} target.

yield of the 475-kev γ rays from Coulomb excitation of Ru^{102}. The γ-ray yields given in Table I have been corrected for the presence of the 478-kev γ rays from $Li(p,p')$. This correction amounted to 5% at $E_p=3.0$ Mev.

Coulomb excitation of Ru^{96} and Ru^{98} has not previously been reported. No information on the excited states of Ru^{96} is available from radioactive decay studies. The decay of both Tc^{98} and Rh^{98} to Ru^{98} results in the emission of 650-kev γ rays[20,21] which agrees with the level position of 654 kev found from Coulomb excitation.

Temmer and Heydenburg[19] have reported energies and $B(E2)_{ex}$ for Ru^{104}, Ru^{102}, and Ru^{100}; the latter being

[20] G. E. Boyd and Q. V. Larson, J. Phys. Chem. 60, 707 (1956).
[21] S. Katcoff and H. Abrash, Phys. Rev. 103, 966 (1956).

assigned on the basis of systematics. The agreement as to the positions of the levels is good. It is difficult to judge how well the values for $B(E2)_{ex}$ compare, since they do not give explicit errors. Our relative values are considerably different from theirs. For example, we find the ratio of the $B(E2)_{ex}$ for Ru^{104} to Ru^{100} is 1.62 ±0.11 whereas their value is 3.5.

D. Palladium $(Z=46)$.—Figures 10 to 13 show representative spectra for proton bombardment of enriched targets of Pd^{104}, Pd^{106}, Pd^{108}, and Pd^{110}. The 440-kev γ ray from $Na(p,p'\gamma)$ is present in the palladium spectra and this γ ray intefers with the determination of the yield of the 433-kev γ ray from Coulomb excitation of Pd^{108}. We have applied a correction by taking the average value for the intensity of the 440-kev sodium γ ray observed in the other palladium spectra and subtracting this from the yield of the Pd^{108} γ ray. A

FIG. 15. Pulse-height spectrum for protons on Cd^{108} target.
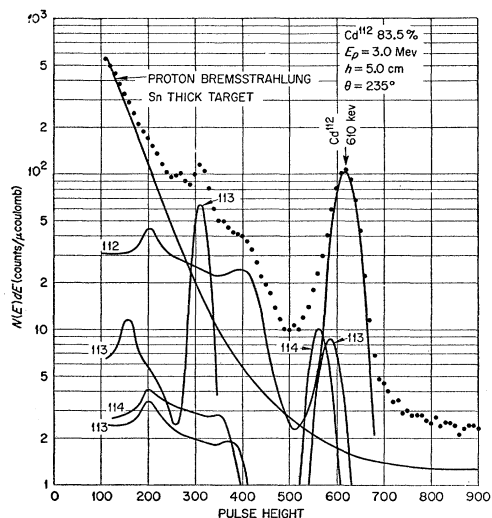

FIG. 13. Pulse-height spectrum for protons on Pd^{110} target.

FIG. 14. Pulse-height spectrum for protons on Cd^{106} target.

FIG. 16. Pulse-height spectrum for protons on Cd^{110} target.

concentration of approximately 300 ppm by weight of sodium in the target is indicated by the intensity of the 440-kev γ ray. The correction at 3.0-Mev proton energy amounted to 4%. Temmer and Heydenburg have also measured the Coulomb excitation of the four even-even isotopes of palladium.[19] Here, also, there is a considerable divergence in the relative values of the $B(E2)_{ex}$. For instance, we find the ratio of the $B(E2)_{ex}$ for Pd^{110} to Pd^{104} is 1.57±0.10 whereas their ratio is 2.26.

E. Cadmium $(Z=48)$.—γ-ray spectra resulting from proton Coulomb excitation of targets enriched in Cd^{106}, Cd^{108}, Cd^{110}, Cd^{112}, Cd^{114}, and Cd^{116} and normal Cd, respectively, are shown in Figs. 14 to 20. The percentage abundance of Cd^{106} and Cd^{108} in the enriched samples was not very favorable because of the low natural abundance of these isotopes. The situation is made

still more difficult by the superposition of the γ ray of the other isotopes on those of Cd^{106} and Cd^{108}. Consequently the errors on the γ-ray yields for Cd^{106} and Cd^{108} are considerably larger than those for the other isotopes. Coulomb excitation of Cd^{106} and Cd^{108} has not previously been reported. Nothing is known about excited states of Cd^{106} from radioactive decay. The decay of both Ag^{108} and In^{108} to Cd^{108} [22] results in the emission of a γ ray which has an energy in agreement with the 630 ± 10 kev determined from Coulomb excitation.

As indicated in Table I, the yield of the 555-kev γ ray from Cd^{114} was also measured for 9-Mev α-particle

FIG. 17. Pulse-height spectrum for protons on Cd^{112} target.
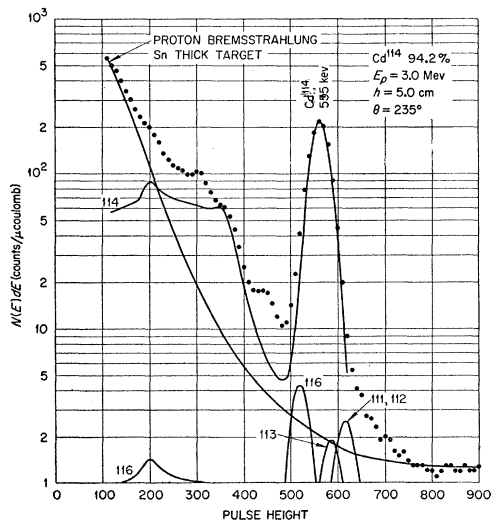
FIG. 18. Pulse-height spectrum for protons on Cd^{114} target.

[22] W. Mead, University of California Radiation Laboratory Report UCRL-3488, 1956 (unpublished); Perlman, Bernstein, and Schwartz, Phys. Rev. 92, 1236 (1953); M. C. Joslin and B. V. Thosan, Proc. Indian Acad. Sci. 43A, 255 (1956).
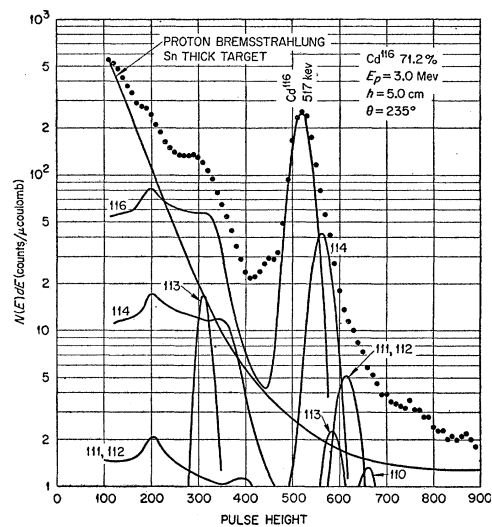

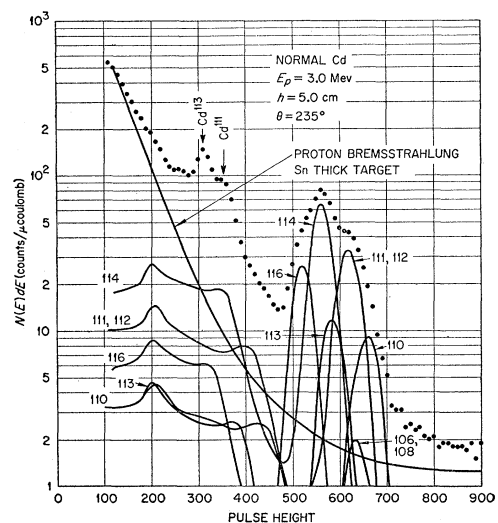FIG. 19. Pulse-height spectrum for protons on Cd^{116} target.

FIG. 20. Pulse-height spectrum for protons on normal cadmium target.

bombardment to check that the $B(E2)_{ex}$ obtained from proton and α-particle excitation are consistent. The average value of the $B(E2)_{ex}$ obtained with protons and that obtained with α particles differ by 4%. This difference is believed to be reasonable in view of the facts (a) that a 3 in.$\times$3 in. NaI crystal was used for the α-particle work whereas a $1\frac{1}{2}$ in.$\times$1 in. crystal was used in the earlier proton work, and (b) that the relation used to convert from proton stopping power to α-particle stopping power is probably not strictly valid.

Temmer and Heydenburg[19] have reported Coulomb excitation of Cd^{110}, Cd^{112}, Cd^{114}, and Cd^{116}. Our values for the level positions agree, to within the assigned errors, with their values. We find the ratios of the $B(E2)_{ex}$ for Cd^{116} to Cd^{110} and Cd^{116} to Cd^{112} are 1.19

±0.08 and 1.11±0.07, respectively, whereas they obtained the somewhat larger values of 1.51 and 1.35.

F. Tin (Z=50).—Figures 21, 22, and 23 show spectra for 10-Mev α-particle excitation in targets of normal Sn and enriched Sn^{116}, Sn^{118}, Sn^{120}, Sn^{122}, and Sn^{124}. The spectra indicate excitation of numerous other γ rays in addition to those assigned to Coulomb excitation of the 2^+ states of the even-even tin isotopes. The origins of some of these γ rays have been determined and these are identified in the figures. Most of those which have not been identified are believed to result from reactions
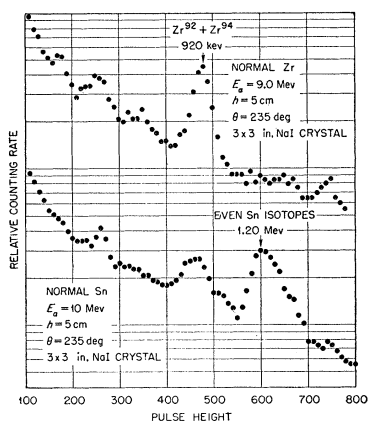
FIG. 21. Pulse-height spectra for α particles on normal zirconium and normal tin targets.
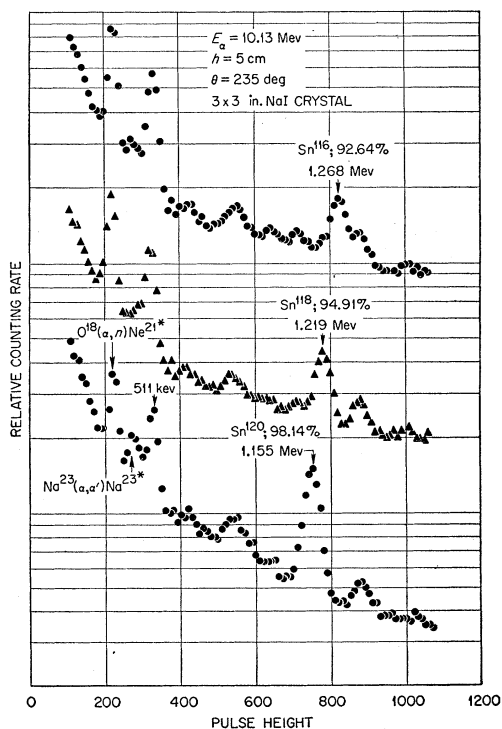

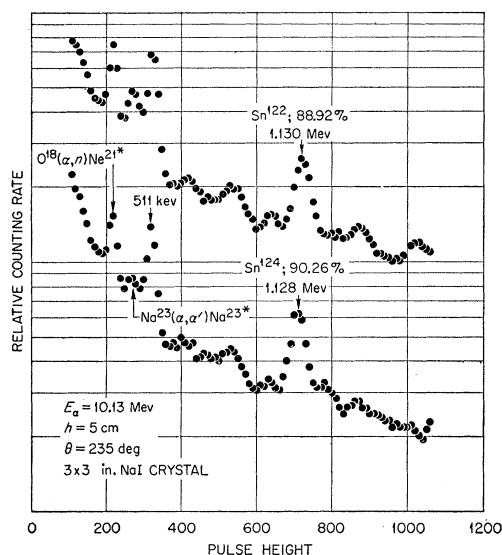FIG. 22. Pulse-height spectra for α particles on Sn^{116}, Sn^{118}, and Sn^{120} targets.

FIG. 23. Pulse-height spectra for α particles on Sn^{122} and Sn^{124} targets.

produced in small amounts of low-Z target impurities. Alkhazov *et al.*[23] have studied Coulomb excitation of Sn^{117} and Sn^{119} and they find γ rays of 865 and 1030 kev in Sn^{117} and 907 kev in Sn^{119}. These γ rays could account for the broad peak at 470 pulse-height units observed in the spectrum for normal tin.

The angular distribution of the 1155-kev γ rays excited in the Sn^{120} target was measured to be $1+(0.29\pm0.02)P_2-(0.04\pm0.03)P_4$ for an α-particle energy of 10 Mev. The expected angular distribution for the Coulomb excitation of a 2^+ state under these experimental conditions is $1+0.30P_2-0.09P_4$.

The locations of the first excited states of Sn^{116}, Sn^{120}, and Sn^{122} are known from radioactive-decay studies. The first excited state of Sn^{118} and Sn^{124} were not previously known. From the decay of In^{116}, Slätis *et al.*[24] determined the energy of the first excited state of Sn^{116} to be (1274±6) kev and this agrees well with our value of (1268±10) kev. McGinnis[25] has determined the energy of the first excited state of Sn^{120} to be 1180 kev from the study of the decay of Sb^{120}. From measurements on the decay of Sb^{122} both Farrelly *et al.*[26] and Glaubman[27] have determined the energy of the 2^+ state in Sn^{122} to be (1137±6) kev and (1152±15) kev, respectively, and these values agree with our value of (1130±10) kev.

We have been informed by private communication of work by Alkhazov *et al.*[23] in which Coulomb excitation of the even-even isotopes of tin has been measured.

[23] Private communication from Alkhazov, Lemberg, Andreev, and Erokhina of the Leningrad Physico-Technical Institute, U.S.S.R.
[24] Slätis, Dutoit, and Siegbahn, Arkiv Fysik **2**, 321 (1950).
[25] C. L. McGinnis, Phys. Rev. **98**, 1172(A) (1955).
[26] Farrelly, Koerts, Benczer, van Lieshout, and Wu, Phys. Rev. **99**, 1440 (1955).
[27] M. J. Glaubman, Phys. Rev. **98**, 645 (1955).
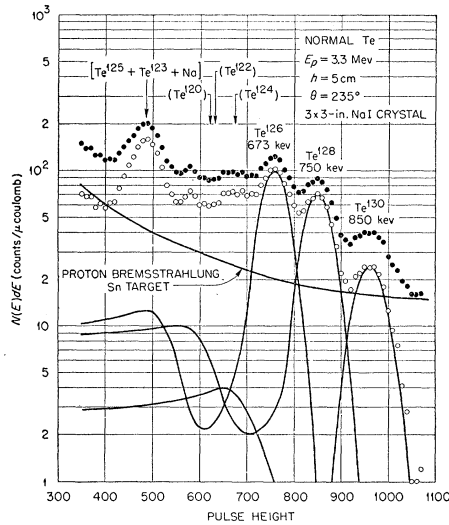
FIG. 24. Pulse-height spectrum for protons on normal tellurium target.

Their values for the energies of the 2⁺ states and the $B(E2)_{ex}$ values are in reasonable agreement with our results.

G. Tellurium $(Z=52)$.—The γ-ray pulse-height spectrum observed when a normal tellurium target was bombarded by 3.3-Mev protons is shown in Fig. 24. Targets of enriched isotopic abundance were not used; others have studied the Coulomb excitation of tellurium with enriched targets.[19] The use of a normal tellurium target limited the isotopes in which Coulomb excitation could be studied to Te^{126}, Te^{128}, and Te^{130}. The positions in the pulse-height spectrum of other weak, unresolved γ rays are indicated by arrows. Coulomb excitation of normal tellurium was also measured with 9- and 10-Mev α particles and the resulting γ-ray yields were more precisely determined than those for proton excitation because the background was much lower with α-particle excitation. The values for $B(E2)_{ex}$ obtained with proton and α-particle excitation (see Table I) are in satisfactory agreement.

Information on the location of the 2⁺ state in Te^{130} is not available from radioactive decay work. Our value of 850 kev is in good agreement both with other Coulomb excitation results[19] and with the value of 830 ± 20 kev obtained by Sinclair from the (n,n') reaction.[28]

Benczer et al.[29] have established that the 2⁺ state of Te^{128} is excited in the decay of I^{128}. Their value for the energy of 750 ± 7 kev compares well with the Coulomb excitation result of Heydenburg and Temmer (750 kev)[19]; the (n,n') result of Sinclair (760 ± 20) kev[28]; and with our result of (750 ± 10) kev.

Several values are available for the energy of the 2⁺ state of Te^{126} but here the agreement is not quite so

²⁸ R. M. Sinclair, Phys. Rev. 102, 461 (1956).
²⁹ Benczer, Farrelly, Koerts, and Wu, Phys. Rev. 101, 1027 (1956).

good. From the radioactive decay of I^{126}, Marty et al. find 670 kev[30]; Perlman and Welker find 651 ± 10 kev[31]; and Koerts et al. find 650 ± 10 kev.[32] From Coulomb excitation, Heydenburg and Temmer obtain 662 kev,[19] and from (n,n') Sinclair finds 680 ± 20 kev.[28] Our value is 673 ± 7 kev.

Our values for the $B(E2)_{ex}$ for Te^{126}, Te^{128}, and Te^{130} are not in good agreement with those obtained by Heydenburg and Temmer. Their absolute values are considerably smaller than ours and the ratios of the $B(E2)_{ex}$ for the different isotopes differ somewhat from those we obtain. For instance, we find that the ratio of the $B(E2)_{ex}$'s for Te^{126} to Te^{130} is 1.56 ± 0.13 whereas they obtain 1.23.

V. COMPOUND NUCLEUS REACTIONS

The above discussion of the errors involved in the determination of the values of $B(E2)_{ex}$ assumed that the observed γ-ray yields resulted solely from Coulomb excitation. In this section we wish to investigate the validity of this assumption by considering (a) the comparison of the experimental results with the theory of Coulomb excitation and (b) the magnitude of the
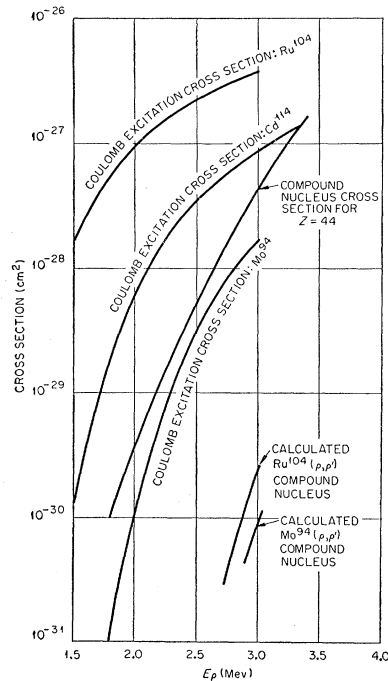

FIG. 25. Cross sections for Coulomb excitation by protons of the 358-kev state in Ru^{104}, the 555-kev state in Cd^{114} and the 874-kev state in Mo^{94}. The calculated cross section for compound nucleus formation for ruthenium $(Z=44)$ is shown. The calculated cross sections for excitation of the 358-kev state of Ru^{104} and the 874-kev state in Mo^{94} by compound-nucleus inelastic proton scattering are also shown.

³⁰ Marty, Langevin, and Hubert, Compt. rend. 236, 1153 (1953).
³¹ M. L. Perlman and J. Welker, Phys. Rev. 95, 133 (1954).
³² Koerts, Macklin, Farrelly, van Lieshout, and Wu, Phys. Rev. 98, 1230 (1955).

γ-rays yields to be expected from the alternative mechanism of compound nucleus inelastic proton or α-particles scattering.

For most of the nuclei studied, the γ-ray yields were observed over a considerable range of projectile energies. In some cases, both protons and α particles were used to excite a given state. When the variations in yield are compared to those predicted by the theory of Coulomb excitation, good agreement is found for most of the nuclei. Significant discrepancies were found in three cases, but these discrepancies are reasonably accounted for by the interference from γ rays produced by reactions in the small amounts of light element impurities in the targets. Angular distributions of the γ rays have been measured for a range of projectile energies for several of the nuclei and to within experimental error these distributions agree with those expected for Coulomb excitation.[14] However, these arguments based on the agreement between experiment and theory of the yields and angular distributions are somewhat weakened by the fact that the most accurate experimental results are for those nuclei which exhibit the strongest excitation whereas possible interference from compound nucleus reactions should be most important for those cases in which the cross sections are the smallest. With reference to Fig. 25, it is seen that for a given projectile energy the observed cross sections may differ by a factor of 100 or more for different nuclei (see Ru^{104} and Mo^{94}).

Measured values of relevant cross sections for compound nucleus inelastic scattering cross sections, $[\sigma(x,x')]_{\mathrm{comp}}$, do not exist. The first step in the theoretical estimate of such cross sections is the estimate of the cross section for formation of the compound nucleus, σ_{comp}. Recently, some experimental information on σ_{comp} for protons on medium weight nuclei has been obtained from the study of (p,n) reactions.[33,34] These cross sections were found to be fairly well accounted for by straightforward theoretical estimates based on barrier penetrabilities. As a result, for protons on the nuclei in which we are interested, σ_{comp} may be estimated to within a factor of 2. The estimated cross section for ruthenium $(Z=44)$ as a function of proton energy is shown in Fig. 25. Estimates of σ_{comp} for α particles on medium weight nuclei are considerably more uncertain than those for protons. The interaction radius is not well known because of the lack of experimental information. Theoretical estimates of σ_{comp} given by Blatt and Weisskopf[35] for tin $(Z=50)$ for two possible interaction radii are shown as a function of α-particle energy in Fig. 26. Probably a factor of 10 uncertainty exists in the estimates of σ_{comp} for α particles.

The values for σ_{comp} may be taken as an upper limit for the excitation of the 2$^+$ by $[\sigma(x,x')]_{\mathrm{comp}}$. A com-

[33] Johnson, Galonsky, and Ulrich, Phys. Rev. **109**, 1232 (1958).
[34] J. P. Schiffer and L. L. Lee, Jr., Phys. Rev. **107**, 640 (1957).
[35] J. M. Blatt and V. F. Weisskopf, *Theoretical Nuclear Physics* (John Wiley and Sons, Inc., New York, 1952).
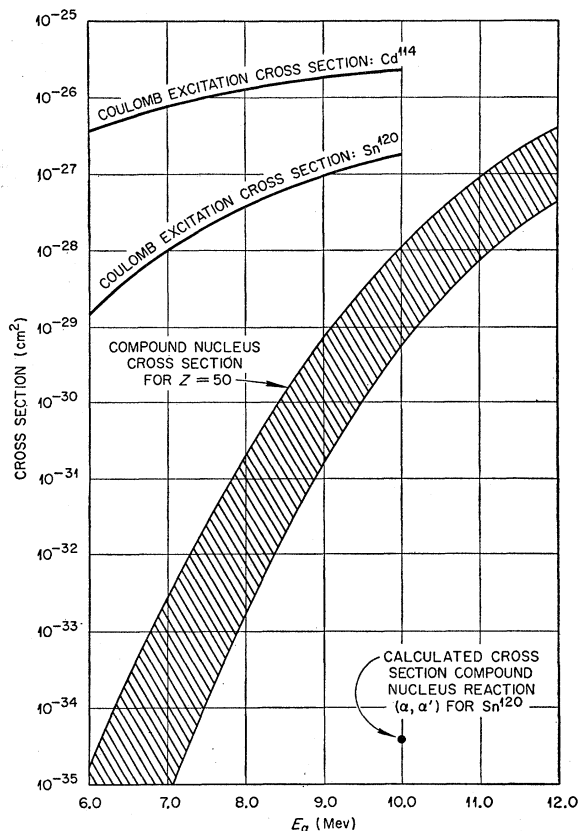
FIG. 26. Cross sections for the Coulomb excitation by α particles of the 1155-kev state in Sn^{120} and the 555-kev state in Cd^{114}. The calculated cross section for compound nucleus formation by α particles on Sn is indicated by the cross-hatched band. The calculated cross section for the excitation of the 1155-kev state in Sn^{120} by compound-nucleus inelastic α-particle scattering at 10-Mev is also shown.

parison of the cross sections for protons presented in Fig. 25 shows that σ_{comp} is never more than a few percent of the cross section for Coulomb excitation of Ru^{104}. On the other hand, σ_{comp} is actually larger than the cross section for Coulomb excitation of Mo^{94}. As one would expect, the situation is improved for α particles; the relatively small cross section for Coulomb excitation of Sn^{120} is still at least 10 times larger than σ_{comp}.

To obtain estimates of $[\sigma(x,x')]_{\mathrm{comp}}$ it is next necessary to estimate the relative probabilities for the different possible modes of decay for the states of the compound nucleus. If the excitation energy of the compound nucleus is above the threshold for neutron emission, this mode of decay will generally be dominant. However, we omit the consideration of neutron emission, since, if it exists, it serves to reduce still further the expected values of $[\sigma(x,x')]_{\mathrm{comp}}$. We restrict the possible modes of decay of the compound states to radiative capture (partial width Γ_γ), and to re-emission of charged particles which either leave the residual nucleus in the ground state (partial width Γ_x) or in the first 2$^+$ excited state (partial width $\Gamma_{x'}$). According to

the theory of nuclear reactions, one expects the charged particle widths, Γ_x and $\Gamma_{x'}$, to be equal to $T_l(x$ or $x')$ $\times D_J/2\pi$, where T_l is the barrier penetration factor and D_J is the average spacing of states with spin J at the excitation energy of the compound nucleus. Therefore, if one has values for D_J he can obtain Γ_x and $\Gamma_{x'}$ for each type of compound state, i.e., given spin and parity. Newton's formula[36] was used to obtain values of D_J.[37] The radiation widths, Γ_γ, were calculated by the use of Cameron's formula.[38] This formula is based on Newton's level spacing formula and assumes dipole emission. It also contains a constant which was adjusted to give a good fit to observed neutron capture radiation widths.

The calculated values for $[\sigma(x,x')]_{\text{comp}}$ are shown in Figs. 25 and 26 for 2.7- and 3.0-Mev protons on Ru^{104}, 3.0-Mev protons on Mo^{94}, and for 10-Mev α particles on Sn^{120}. It is difficult to judge the reliability of these estimates of $[\sigma(x,x')]_{\text{comp}}$ because not enough is known about the general reliability of Newton's formula for the level spacing and of Cameron's formula for the width for radiative capture. The salient result of these estimates is that in each case $[\sigma(x,x')]_{\text{comp}}$ is much less than σ_{comp}. The predominant mode of decay for the compound states is by radiative capture. These estimates suggest that interference from $[\sigma(x,x')]_{\text{comp}}$ for the proton and α-particle energies employed in the present experiments introduces a negligible error in the determination of Coulomb excitation cross sections. For the case of the very weak Coulomb excitation of Mo^{94}, the calculated contribution to the γ-ray yield from $[\sigma(x,x')]_{\text{comp}}$ is less than 1%.

VI. DISCUSSION

In column 8 of Table II we list the ratio of the observed $B(E2)_d$ to that expected for a transition between states of the single-particle model. We have taken $B(E2)_{\text{sp}}$ to be equal to $(1/4\pi)|\frac{3}{5}R_0^2|^2$ where $R_0=1.20\times10^{-13}A^{\frac{1}{3}}$ cm.[35]

The even-even tin isotopes present an interesting situation. The protons in these nuclei, having completed the major shell at 50, should make these nuclei quite rigid. The large excitation energy of the 2+ states is compatible with this view and one might have expected that the transition rates would be those given by $B(E2)_{\text{sp}}$. However, the observed rates are approximately 13 times larger. Although the protons form a closed shell, the neutron numbers for the tin isotopes are about midway between the major shells of 50 and 82. Consequently one would expect the neutrons to exert a deforming or softening action on the nuclei and perhaps the enhanced transition rates reflect this action.

The energy of the first excited state of even-even

medium weight nuclei shows a strong variation with changes in neutron and proton number. Although the over-all trend is a smooth decrease in excitation energy with removal from closed shells, some interesting exceptions to this behavior have appeared. The anomalous behavior of Mo^{96} and Mo^{98} has been reported[19] and we confirm this result. The cadmium isotopes are also exceptional. The four heaviest isotopes establish a trend with neutron number which, if continued by Cd^{108} and Cd^{106}, would place the excited states above that for Cd^{110} (656-kev) whereas both isotopes have excited states at 630-kev. The variation in excitation energies with proton number clearly indicates the unusual stability of the 40-proton configuration. The relatively small value for the transition rate of Zr^{92} and and Zr^{94} probably results from the combined effects of neutron numbers near to 50 and the increased stability of the 40-proton configuration.

The values for $B(E2)_{\text{ex}}$ also show strong and fairly systematic trends with variations in neutron and proton number. The plot of the observed $B(E2)_{\text{ex}}$ vs neutron number is given in Fig. 27. A close correlation is found between the $B(E2)_{\text{ex}}$ and the excitation energy of a given state. To exhibit this we have also plotted in Fig. 27 the quantity $3.24/E_{2+}(\text{Mev})$. The constant 3.24 was chosen to give a good fit to those nuclei with large $B(E2)_{\text{ex}}$. The anomalous behavior of the excitation energies for the molybdenum isotopes is also reflected in the values for $B(E2)_{\text{ex}}$.

In order to more clearly demonstrate the observed dependence of the $B(E2)_{\text{ex}}$ on the energy of the excited state, a plot of $\log B(E2)_{\text{ex}}$ vs $\log E_{2+}$ is given in Fig. 28. The straight line in the figure has a slope of -1, corresponding to a E^{-1} energy dependence.
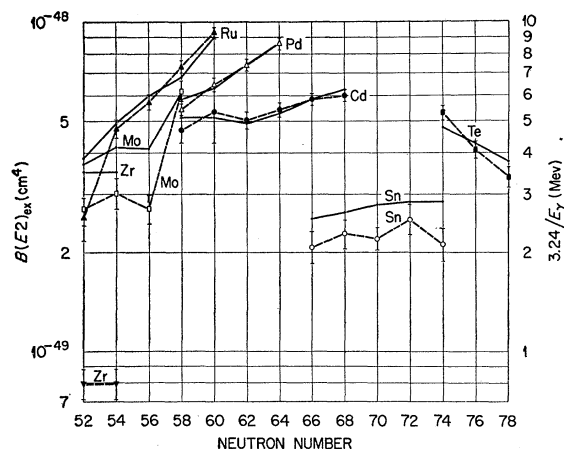

FIG. 27. Plot of the experimental values for $B(E2)_{\text{ex}}$ vs neutron number. The values for $B(E2)_{\text{ex}}$ (referred to the left-hand ordinate) are designated by different symbols for different elements. To demonstrate the close correlation between the $B(E2)_{\text{ex}}$ and the energy of the 2+ state, we have also plotted the quantity $3.24/E_{2+}(\text{Mev})$ vs neutron number. These values, which are connected by solid lines for a given element, refer to the right-hand ordinate.

[36] T. D. Newton, Can. J. Phys. 34, 804 (1956).

[37] Excitation energies of the compound nucleus were calculated by the use of mass values given by A. H. Wapstra, Physica 21, 385 (1955).

[38] A. G. W. Cameron, Can. J. Phys. 35, 666 (1957).

Two types of collective motion have been proposed to account for "near harmonic" spectra; the free oscillation of a nucleus about the spherical shape,[4,15] and the "γ unstable" motion.[6] From the $B(E2)_{ex}$ and the E_{2+} one obtains the parameters B_2 and C_2 which are appropriate to the description of quadrupole vibrations about the spherical shape.[19,15] C_2 represents the effective surface tension and B_2 represents the mass transported by the collective motion. Formulas (6) show the relation between these quantities:

$$C_2(\text{Mev}) = 0.995 Z^2 E_{2+}(\text{Mev})/$$
$$[B(E2)_d/B(E2)_{sp}], \quad (6a)$$

$$B_2/(B_2)_{irrot} = \frac{241(Z^2/A^{5/3})}{E_{2+}(\text{Mev})[B(E2)_d/B(E2)_{sp}]}. \quad (6B)$$

The value $(B_2)_{irrot}$ is that expected for the case of irrotational flow. The values for C_2 and $B_2/(B_2)_{irrot}$ are listed in Table II. Of the two experimental quantities, E_{2+} and $B(E2)_d$, which enter into the calculation of the parameter C_2 and $B_2/(B_2)_{irrot}$, the $B(E2)_d$ has the dominant error. Since both parameters vary inversely with $B(E2)_d$, the percentage errors given in Table II as R.E. and A.E. will also be approximately correct for C_2 and $B_2/(B_2)_{irrot}$.

The parameters appropriate to the "shape unstable" model are β and $B_2/(B_2)_{irrot}$, where β is

$$\beta = [2.91 \times 10^{26}][B(E2)_{ex}]^{\frac{1}{2}}/ZA^{\frac{1}{3}}. \quad (7)$$

The values of β are listed in Table II. Since β depends on the square root of $B(E2)_{ex}$, the percentage error
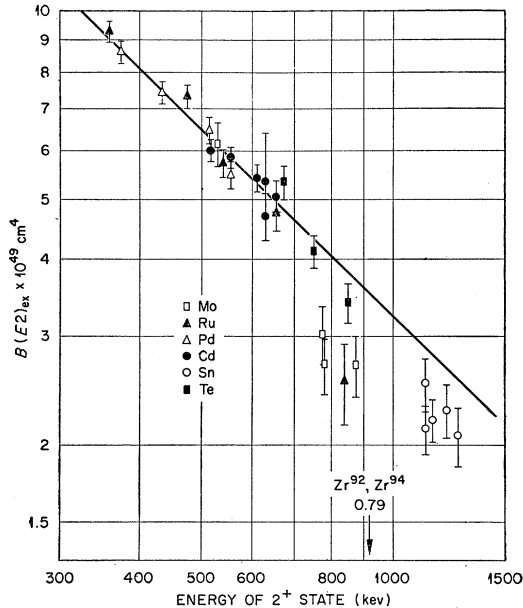

FIG. 28. Plot of $\log B(E2)_{ex}$ vs $\log E_{2+}$. The straight line has a slope of -1 corresponding to a E^{-1} dependence for the $B(E2)_{ex}$.

in β is approximately one half the percentage errors R.E. and A.E.

For those nuclei where the values for C_2 and $B_2/(B_2)_{irrot}$ may be compared to the earlier results of Heydenburg and Temmer,[19] the observed differences result from differences in the experimental values for $B(E2)_{ex}$. In spite of these differences, both sets of values for the parameters point to the rapid variation in C_2 and to large values for $B_2/(B_2)_{irrot}$. Our values for $B_2/(B_2)_{irrot}$ display more uniformity; in fact, the constancy of $B_2/(B_2)_{irrot}$ for a large number of the nuclei is a striking feature. It is also interesting to note that some of the values for β in Table II are as large as those for nuclei which exhibit rotational spectra.

APPENDIX. ENERGY LOSS OF PROTONS IN SILVER AND GOLD

The number of γ rays excited in a target by the Coulomb excitation process is proportional to

$$\int_{E_f}^{E_i} \frac{\sigma(E)dE}{S(E)}, \quad (1)$$

where

$$E_f = E_i - \int_0^x S dx. \quad (2)$$

$\sigma(E)$ is the cross section and $S(E)$ is the energy loss. The shape of the cross section curve as a function of energy for Coulomb excitation has been accurately calculated and has been experimentally confirmed. The absolute value of $\sigma(E)$ depends on $B(E2)_{ex}$. One has that $\sigma(E) = BX(E)$, where $X(E)$ is known. Therefore one has

$$B \propto 1 \bigg/ \int_{E_f}^{E_i} \frac{X(E)dE}{S(E)}.$$

Now, for a thick target $(E_f = 0)$ one sees that if $S(E)$ is uniformly 10% too large then B will be in error by 10%. On the other hand, if the target is sufficiently thin, the error introduced in the integrand is just counteracted by the change in the limit E_f. So, from thin-target measurements on silver and gold, one can get good values of B, even with an error in the value taken for $S(E)$. One then compares these values with those obtained by bombarding thick targets with protons of various incident energies. From this comparison one can deduce the error in $S(E)$ and alter $S(E)$ until yields from thick and thin targets give consistent values for B. It is not necessary to know the γ-ray detection efficiency to high accuracy since it drops out in the comparison of thick and thin targets. However, it is necessary to know quite accurately the thickness x of the thin target, since this enters into the determination of B.

The thin foils were chosen to be only moderately thin because it is desirable to have sufficient Coulomb excita-

TABLE III. $dE/d\rho x$ for protons in Au and Ag.

E_p(Mev)	$_{79}$Au $(dE/d\rho x)_p$ kev/(mg/cm²)	E_p(Mev)	$_{47}$Ag $(dE/d\rho x)_p$ kev/(mg/cm²)
5.0	27.8	3.3	50.7
4.8	28.5	3.2	51.6
4.6	29.2	3.1	52.4
4.4	30.0	3.0	53.4
4.2	30.8	2.9	54.3
4.0	31.6	2.8	55.4
3.8	32.7	2.7	56.4
3.6	33.7	2.6	57.5
3.4	34.9	2.5	58.6
3.2	36.1	2.4	59.7
3.0	37.3	2.3	61.0
2.8	38.7	2.2	62.3
2.6	40.3	2.1	63.7
2.4	42.2	2.0	65.2
2.2	44.4	1.9	66.8
2.0	46.7	1.8	68.5
1.8	49.3	1.7	70.5
1.6	52.3	1.6	72.7
1.4	55.9	1.5	75.1
1.2	60.1	1.4	77.8
1.0	65.1	1.3	80.8
0.8	71.3	1.2	84.1
		1.1	87.9
		1.0	92.5
		0.9	98.0
		0.8	104.0

tion yield to make the yield of the proton bremsstrahlung (from foil and foil backing) small in comparison.

Gold and silver foils in 6×6 in. squares were obtained from Baker and Company, Inc. These were successively cut into smaller squares in order to study the macroscopic uniformity. In this way profiles of the thickness of the original large foils were obtained. Small foils for the experiment were chosen from those sections showing the greatest uniformity. It is judged that the thickness of the foils used is known to 0.5% for the gold foils (thickness ~10 mg/cm²) and to 1.0% for the silver foils (thickness ~6 mg/cm²). The silver foils were mounted on tin backings of approximately 80 mg/cm² thickness, and the gold foils were mounted on bismuth backings of approximately 120 mg/cm² thickness. Both the tin and bismuth backings were prepared by electrodeposition onto 5-mil nickel foils. Three thin targets each of silver and gold were prepared to check the reproducibility of the measurements.

Since the foils are only moderately thin, one expects that the values obtained for B are not completely independent of the values taken for $S(E)$. We have studied this problem in the following way: We assumed that the shape of $S(E)$ was known. We then changed the absolute values by a certain percentage, for example, 10%, and carried out numerical integration to find the resultant change in the thin-target B value for various incident proton energies and for the foil thicknesses used. The ratio of the percentage change in B to the percentage change in $S(E)$ was 0.35 for the worst case (3-Mev protons on gold foil) and 0.08 for the best case (5-Mev protons on gold foil). This ratio is then useful in the determination of the values of $S(E)$ which will give the same B values for thick and thin targets.

Measurements were made at proton energies of 3.0, 3.5, 4.0, 4.5, and 5 Mev for gold and at 2.4, 2.7, 3.0, and 3.3 Mev for silver. Coulomb excitation of the states at 550 and 277 kev in gold and at 419 and 316 kev in silver was studied.

Two small corrections were applied. First, one must take into account the fact that angular distribution of the gamma rays from Coulomb excitation varies (slowly) with the incident proton energy. The angular distributions are known for silver and gold.[39] Appropriate averages over target thickness have been determined and applied to measurements. Second, allowance was made for the fact that the multiple small-angle Rutherford scattering makes the effective path length in the foil somewhat larger than the foil thickness. This increase can be calculated by the use of the theory of Goudsmit and Saunderson[40] and Williams.[41] For our cases it was found that the largest correction for this effect was 0.5% (3-Mev protons on the gold foil).

Our best values for $S(E)$ for silver and gold are given in Table III. These measurements are of an integral type and are useful in obtaining accurate values of B from Coulomb excitation with thick targets. However, they are not suited for a detailed examination of the shape of $S(E)$. Rather, one must assume that he knows the shape of $S(E)$ and then determine whether the experiments are consistent with the assumed shape. Our shape for $S(E)$ for silver is of the form $S(E) \propto E^{-\frac{1}{2}}$, and that for gold is very nearly of this shape. Theoretical consideration and experimental results[42] suggest this energy dependence for $S(E)$. If one accepts the fact that the shapes for $S(E)$ are correct (and the experiments are consistent with these shapes), then it is felt that the absolute values of $S(E)$ are determined to within ±4% (standard deviation).

[39] F. K. McGowan and P. H. Stelson, Phys. Rev. **99**, 127 (1955).
[40] S. Goudsmit and J. L. Saunderson, Phys. Rev. **57**, 24 (1940).
[41] E. J. Williams, Phys. Rev. **58**, 292 (1940).
[42] A. Winther (private communication).